Journal of Turbulence
Volume 7, No. 3, 2006

Taylor & Francis
Taylor & Francis Group

Divergence-free and curl-free wavelets in two dimensions and three dimensions: application to turbulent flows

ERWAN DERIAZ* and VALÉRIE PERRIER

Laboratoire de Modélisation et Calcul de l'IMAG, BP 53-38 041 Grenoble Cedex 9, France

We investigate the use of compactly supported *divergence-free wavelets* for the representation of solutions of the Navier–Stokes equations. After reviewing the theoretical construction of divergence-free wavelet vectors, we present in detail the bases and corresponding fast algorithms for two and three-dimensional incompressible flows. We also propose a new method for practically computing the *wavelet Helmholtz decomposition* of any (even compressible) flow; this decomposition, which allows the incompressible part of the flow to be separated from its orthogonal complement (the gradient component of the flow) is the key point for developing divergence-free wavelet schemes for Navier–Stokes equations. Finally, numerical tests validating our approach are presented.

Keywords: Divergence-free wavelets; Curl-free wavelets; Turbulent flows

1. Introduction

The prediction of fully developed turbulent flows represents an extremely challenging field of research in scientific computing. The *direct numerical simulation* (DNS) of turbulence requires the integration in time of the full nonlinear Navier–Stokes equations, that is the computation of all scales of motion. However, at large Reynolds numbers, turbulent flows generate increasingly small scales; to be realistic, the discretization in space (and also in time) ought to handle a huge number of degrees of freedom. This is impossible with currently available computers in three dimensions.

Many attempts have been made, or are under way, to overcome this problem: among these are *vortex methods* which are able to generate very thin scales, or *large eddy simulations (LES)* and subgrid-scale techniques that separate the flow into large scales, which are explicitly computed, from small scales, that are parameterized or computed statistically.

In this context, wavelet bases offer a different approach. They provide an alternative decomposition, allowing the intermittent spatial structure of turbulent flows to be represented with only a few degrees of freedom. This property comes from the good localization, in both physical and frequency domains, of the basis functions. The wavelet decomposition was *introduced* at the beginning of the 1990s for the analysis of turbulent flows [1–3]. Wavelet based methods for the resolution of the two-dimensional (2D) Navier–Stokes equations appeared later [4–9], and very recently for three-dimensional (3D) domains [10, 11]. They have also been used to define LES-type methods such as the coherent vortex simulation

*Corresponding author. E-mail: Erwan.Deriaz@imag.fr

Journal of Turbulence
ISSN: 1468-5248 (online only)
http://www.tandf.co.uk/journals
DOI: 10.1080/14685240500260547

(CVS) method [12, 37] and adaptive LES methods [13], or to derive 3D models of turbulence [14]. Most of these cited works use a Galerkin, a Petrov–Galerkin or a collocation approach for the *vorticity formulation* in dimension two, with periodic boundary conditions [39]. However, these approaches are not appropriate for the 3D case with non-periodic boundary conditions.

An alternative approach was, at the same period, considered first by Urban and then investigated by several authors. They proposed to use the *divergence-free wavelet bases* originally designed by Lemarié-Rieusset [15, 38]. Divergence-free wavelet vectors have been implemented and used to analyse 2D turbulent flows [16–18], as well as to compute the 2D–3D Stokes solution for the driven cavity problem [19, 20]. Since divergence-free wavelets are constructed from standard compactly supported biorthogonal wavelet bases, they can incorporate boundary conditions [21, 22].

The great interest of divergence-free wavelets is that they provide bases suitable for representing the incompressible Navier–Stokes solution, in two and three dimensions. Our present objective is thus to investigate their practical feasibility and amenability. In order to eliminate the pressure, we project the equations on to the space of divergence-free vectors. This (orthogonal) projection is the well-known Leray projector and can be computed explicitly in Fourier space for periodic boundary conditions. Unfortunately, as already noted by Urban [22], the Leray operator cannot be represented simply in terms of divergence-free wavelets, since they form biorthogonal bases (and not orthogonal).

The goal of the present paper is to investigate the use of divergence-free wavelets for the simulation of turbulent flows. First, in section 2 we review the basic ingredients of the theory of compactly supported divergence-free wavelet vectors, developed by Lemarié-Rieusset [15]. In section 3, we present in detail the bases that we implement in two and three dimensions: isotropic bases, as presented in the previous work [15, 16, 19], but also anisotropic bases, which are easier to implement. We shall see that the choice of the complement wavelet basis is not unique, and this choice induces the values of divergence-free coefficients for compressible flows. We discuss the algorithmic implementation of divergence-free wavelet coefficients in two and three dimensions, leading to fast algorithms (in $O(N)$ operations where N is the number of grid points).

Section 4 is devoted to the Helmholtz decomposition of compressible fields in a wavelet formulation; the method that we present uses the biorthogonal projectors both on divergence-free and on curl-free wavelets. Our method is an iterative procedure, and we shall experimentally prove that it converges. Section 5 addresses the main ingredients of a Galerkin method for the Navier–Stokes equations, based on divergence-free wavelets. Finally, the last section presents numerical tests that validate our approach: nonlinear compressions of 2D–3D incompressible turbulent flows, and the wavelet Helmholtz decomposition of several examples, such as the computation of the divergence-free part and the pressure arising from the nonlinear term of the Navier–Stokes equations.

2. Theory of divergence-free wavelet bases

In this section, we review briefly the construction of divergence-free wavelets. Compactly supported divergence-free vector wavelets were originally designed by Lemarié-Rieusset, in the context of biorthogonal multiresolution analyses (MRAs). For the definition and properties of biorthogonal MRAs and associated wavelets, we refer the reader to appendix A, and to the textbooks in [23–26]. For the theory of divergence-free wavelets, see [15, 20] and the book by Urban [18]. We illustrate the construction with the explicit example of splines of degree 1 and 2.

2.1 *Theoretical grounds for the divergence-free wavelet vectors*

Let us introduce

$$\boldsymbol{H}_{\mathrm{div},0}(\mathbb{R}^n) = \{\boldsymbol{f} \in [L^2(\mathbb{R}^n)]^n; \quad \mathrm{div}\ \boldsymbol{f} \in L^2(\mathbb{R}^n), \quad \mathrm{div}\ \boldsymbol{f} = 0\},$$

the space of divergence-free vector functions in $\mathbb{R}^n$.

The divergence-free wavelets in $[L^2(\mathbb{R}^n)]^n$ defined by Lemarié-Rieusset [15], provide the Riesz bases of $\boldsymbol{H}_{\mathrm{div},0}(\mathbb{R}^n)$. Their construction is based on the existence of two different one-dimensional MRAs of $L^2(\mathbb{R})$ related by differentiation and integration.

Let $(V_j^0)_{j\in\mathbb{Z}}$ be a one-dimensional (1D) MRA, with a differentiable scaling function ϕ_1 (meaning that $V_0^1 = \mathrm{span}\{\phi_1(x-k), k \in \mathbb{Z}\}$), and a wavelet ψ_1; one can build a second MRA $(V_j^1)_{j\in\mathbb{Z}}$ with a scaling function ϕ_0 ($V_0^0 = \mathrm{span}\{\phi_0(x-k), k \in \mathbb{Z}\}$) and a wavelet ψ_0 satisfying

$$\phi_1'(x) = \phi_0(x) - \phi_0(x-1), \qquad \psi_1'(x) = 4\,\psi_0(x). \tag{1}$$

Example: spline scaling functions and wavelets of degree 1 and 2: Biorthogonal splines provide wavelet bases which are regular, compactly supported and easy to implement. The scaling functions of the associated MRA are standard B-spline bases, and the wavelets are constructed easily, by linear combinations of translated B splines. An example of an MRA satisfying equation (1) is given by splines of degree 1 (V_j^0 MRA spaces) and splines of degree 2 (V_j^1 MRA spaces). In both cases we draw the scaling functions ϕ_0 and ϕ_1 and their associated wavelets ψ_0 and ψ_1 with shortest support (figure 1).

The *isotropic* divergence-free wavelets in $\mathbb{R}^n$ are then obtained by suitable combinations of tensor products of the functions ϕ_0, ψ_0, and ϕ_1, ψ_1, fulfilling equation (1). Following [15], there exist $(n-1)(2^n-1)$ vector functions $\Psi^{\varepsilon}_{\mathrm{div},i} \in \boldsymbol{H}_{\mathrm{div},0}(\mathbb{R}^n)$ ($\varepsilon \in \Omega_n^*$ of cardinality 2^n-1, $i \in I_\varepsilon$ of cardinality $n-1$) compactly supported, such that every vector function $\boldsymbol{u} \in \boldsymbol{H}_{\mathrm{div},0}(\mathbb{R}^n)$ can be uniquely expanded:

$$\boldsymbol{u} = \sum_{j\in\mathbb{Z}} \sum_{\varepsilon\in\Omega_n^*} \sum_{i\in\mathbb{I}_\varepsilon} \sum_{\boldsymbol{k}\in\mathbb{Z}^n} d^{\varepsilon}_{\mathrm{div},i,j,\boldsymbol{k}}\ \Psi^{\varepsilon}_{\mathrm{div},i,j,\boldsymbol{k}},$$

with $\Psi^{\varepsilon}_{\mathrm{div},i,j,\boldsymbol{k}}(\boldsymbol{x}) = 2^{\frac{nj}{2}} \Psi^{\varepsilon}_{\mathrm{div},i}(2^j\boldsymbol{x} - \boldsymbol{k})$.

The generating wavelets $\Psi^{\varepsilon}_{\mathrm{div},i}$ take the general following form in $\mathbb{R}^n$. Let $\varepsilon \in \Omega_n^* = \{0,1\}^n \setminus \{(0,\ldots,0)\}$ be given. We have to fix an integer $i_0 \in \{1,..,n\}$ such that $\varepsilon_{i_0} = 1$. Then, for every

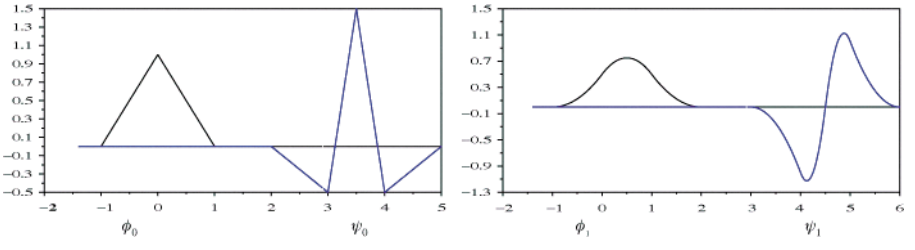

Figure 1. Scaling functions and associated even and odd wavelets with shortest support, for splines of degree 1 (left) and degree 2 (right).

$i \in \{1, \ldots, n\} \setminus \{i_0\}$, the vector function $\Psi^{\varepsilon}_{\text{div},i} = \left(\left[\Psi^{\varepsilon}_{\text{div},i}\right]_\ell\right)_{\ell=1,n}$ can be written

$$\left[\Psi^{\varepsilon}_{\text{div},i}\right]_\ell = \begin{cases} 0 & \text{if } \ell \notin \{i, i_0\}, \\ \gamma^{((i))}_{\varepsilon} & \text{if } \ell = i, \\ \eta_1 \otimes \ldots \otimes \eta_n & \text{if } \ell = i_0, \end{cases} \tag{2}$$

where

$$\gamma^{((i))}_{\varepsilon} = \theta_{0,\varepsilon_1} \otimes \ldots \otimes \theta_{0,\varepsilon_{i-1}} \otimes \theta_{1,\varepsilon_i} \otimes \theta_{0,\varepsilon_{i+1}} \otimes \ldots \otimes \theta_{0,\varepsilon_n}$$

and

$$\begin{aligned} \eta_j &= \theta_{0,\varepsilon_j}, \quad j \neq i, i_0, \\ \eta_{i_0} &= \frac{1}{4}\psi_1, \\ \eta_i &= -\frac{d}{dx}(\theta_{1,\varepsilon_i}), \end{aligned}$$

with the notation

$$\theta_{r,\varepsilon_j} = \begin{cases} \phi_r & \text{if } \varepsilon_j = 0, \\ \psi_r & \text{if } \varepsilon_j = 1, \end{cases}$$

r being equal to 0 or 1.

Example: The 2D *divergence-free vector scaling function* takes the form

$$\Phi_{\text{div}}(x_1, x_2) = \begin{vmatrix} \phi_1(x_1)\phi_1'(x_2) \\ -\phi_1'(x_1)\phi_1(x_2) \end{vmatrix} = \begin{vmatrix} \phi_1(x_1)\,[\phi_0(x_2) - \phi_0(x_2 - 1)] \\ -[\phi_0(x_1) - \phi_0(x_1 - 1)]\,\phi_1(x_2) \end{vmatrix},$$

and the corresponding *isotropic* vector wavelets are given by the system

$$\Psi^{(1,0)}_{\text{div}}(x_1, x_2) = \begin{vmatrix} -\frac{1}{4}\psi_1(x_1)[\phi_0(x_2) - \phi_0(x_2 - 1)] \\ \psi_0(x_1)\phi_1(x_2) \end{vmatrix},$$

$$\Psi^{(0,1)}_{\text{div}}(x_1, x_2) = \begin{vmatrix} \phi_1(x_1)\psi_0(x_2) \\ -\frac{1}{4}[\phi_0(x_1) - \phi_0(x_1 - 1)]\psi_1(x_2) \end{vmatrix},$$

$$\Psi^{(1,1)}_{\text{div}}(x_1, x_2) = \begin{vmatrix} \psi_1(x_1)\psi_0(x_2) \\ -\psi_0(x_1)\psi_1(x_2) \end{vmatrix}.$$

We display in figure 2 the three generating vector wavelets in the case of spline generators of degree 1 and 2 of figure 1.

These wavelets have already been studied by several workers for the analysis of 2D turbulent flows [16, 17], and also to solve the Stokes problem in two and three dimensions [19, 20, 22].

From now on, we shall focus on the 2D and the 3D case, and we shall present the associated fast algorithms. We shall then point out that the expansion of compressible flows following the divergence-free wavelet bases is not uniquely given. Moreover, we shall introduce 2D and 3D *anisotropic* divergence-free wavelets that are easier to implement.

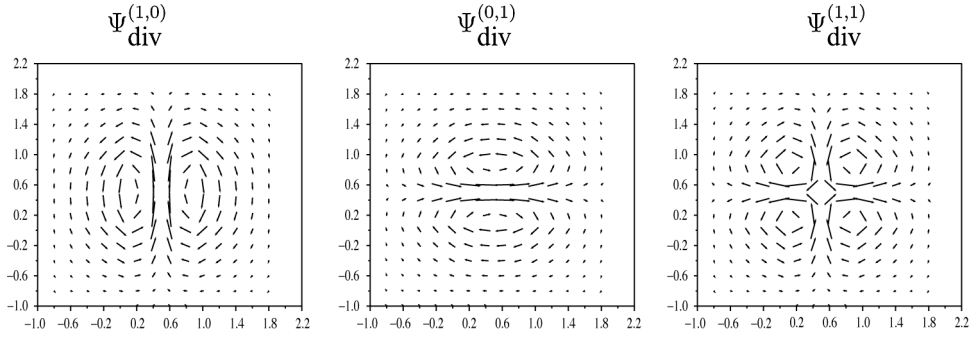

Figure 2. Example of isotropic two-dimensional generating divergence-free spline wavelets $\Psi_{\text{div}}^{(1,0)}$ (left), $\Psi_{\text{div}}^{(0,1)}$ (centre) and $\Psi_{\text{div}}^{(1,1)}$ (right).

3. Isotropic and anisotropic divergence-free wavelets: practical implementation

Isotropic 2D–3D divergence-free wavelet transforms have already been implemented by Urban [18, 20], from divergence-free scaling coefficients. Since the computation of divergence-free scaling coefficients requires the solution of a linear system, we shall propose a different method.

We present in detail our 2D–3D divergence-free wavelet decomposition algorithm; it is based on the construction of a non-unique complement vector space. We also introduce *anisotropic* divergence-free wavelet bases, and their corresponding decomposition algorithms, which differ from previous studies.

In the following, we suppose that we are given two 1D MRAs (V_j^0) and (V_j^1) and ϕ_0, ψ_0 and ϕ_1, ψ_1 their associated (1D) scaling functions and wavelets, satisfying condition (1).

3.1 *Isotropic divergence-free wavelet transforms*

3.1.1 The two-dimensional case. The starting point of the construction is a 2D MRA of $[L^2(\mathbb{R}^2)]^2$:

$$\left(V_j^1 \otimes V_j^0\right) \times \left(V_j^0 \otimes V_j^1\right)$$

whose *2D vector scaling functions* Φ_1 and Φ_2 are given by

$$\Phi_1(x_1, x_2) = \begin{vmatrix} \phi_1(x_1)\phi_0(x_2) \\ 0 \end{vmatrix}, \quad \Phi_2(x_1, x_2) = \begin{vmatrix} 0 \\ \phi_0(x_1)\phi_1(x_2) \end{vmatrix}.$$

In the isotropic case, the six canonical generating *2D vector wavelets* Ψ_i^ε of this MRA are

$$\begin{aligned}
\Psi_1^{(1,0)}(x_1, x_2) &= \begin{vmatrix} \psi_1(x_1)\phi_0(x_2) \\ 0 \end{vmatrix}, & \Psi_2^{(1,0)}(x_1, x_2) &= \begin{vmatrix} 0 \\ \psi_0(x_1)\phi_1(x_2) \end{vmatrix}, \\
\Psi_1^{(0,1)}(x_1, x_2) &= \begin{vmatrix} \phi_1(x_1)\psi_0(x_2) \\ 0 \end{vmatrix}, & \Psi_2^{(0,1)}(x_1, x_2) &= \begin{vmatrix} 0 \\ \phi_0(x_1)\psi_1(x_2) \end{vmatrix}, \\
\Psi_1^{(1,1)}(x_1, x_2) &= \begin{vmatrix} \psi_1(x_1)\psi_0(x_2) \\ 0 \end{vmatrix}, & \Psi_2^{(1,1)}(x_1, x_2) &= \begin{vmatrix} 0 \\ \psi_0(x_1)\psi_1(x_2) \end{vmatrix}.
\end{aligned} \tag{3}$$

Following wavelet theory, the family

$$\left\{\Psi^{\varepsilon}_{i,j,\boldsymbol{k}}(x_1,x_2)=2^j\Psi^{\varepsilon}_i\left(2^jx_1-k_1,2^jx_2-k_2\right)\right\}$$

with $j\in\mathbb{Z}, \boldsymbol{k}=(k_1,k_2)\in\mathbb{Z}^2$, $\varepsilon\in\{(0,1),(1,0),(1,1)\}$, $i=1,2$, forms a basis of $[L^2(\mathbb{R}^2)]^2$. Then a velocity field $\boldsymbol{u}=(u_1,u_2)$ in $[L^2(\mathbb{R}^2)]^2$ has the following wavelet decomposition:

$$\begin{aligned}\boldsymbol{u}=&\sum_{j\in\mathbb{Z}}\sum_{\boldsymbol{k}\in\mathbb{Z}^2}\left(d^{(1,0)}_{1,j,\boldsymbol{k}}\,\Psi^{(1,0)}_{1,j,\boldsymbol{k}}+d^{(1,0)}_{1,j,\boldsymbol{k}}\,\Psi^{(0,1)}_{1,j,\boldsymbol{k}}+d^{(1,1)}_{1,j,\boldsymbol{k}}\,\Psi^{(1,1)}_{1,j,\boldsymbol{k}}\right.\\&\left.+d^{(1,0)}_{2,j,\boldsymbol{k}}\,\Psi^{(1,0)}_{2,j,\boldsymbol{k}}+d^{(0,1)}_{2,j,\boldsymbol{k}}\,\Psi^{(0,1)}_{2,j,\boldsymbol{k}}+d^{(1,1)}_{2,j,\boldsymbol{k}}\,\Psi^{(1,1)}_{2,j,\boldsymbol{k}}\right).\end{aligned}\tag{4}$$

Note that the first line of the decomposition represents the wavelet decomposition in the MRA $(V^1_j\otimes V^0_j)$ of the first component u_1, whereas the second line concerns the wavelet decomposition of u_2 in the MRA $(V^0_j\otimes V^1_j)$.

Isotropic generating divergence-free wavelets are then constructed by linear combination of the Ψ^{ε}_i. More precisely, for each $\varepsilon\in\{(0,1),(1,0),(1,1)\}$, the divergence-free wavelet $\Psi^{\varepsilon}_{\mathrm{div}}$ is given uniquely (and follows the general form (2)), whereas one has to build a complement function Ψ^{ε}_n such that

$$\mathrm{span}\left\{\Psi^{\varepsilon}_1,\Psi^{\varepsilon}_2\right\}=\mathrm{span}\left\{\Psi^{\varepsilon}_{\mathrm{div}}\right\}\oplus\ \mathrm{span}\left\{\Psi^{\varepsilon}_n\right\}.$$

The choice of the functions Ψ^{ε}_n is not unique. Moreover they cannot be constructed such that the space $\mathrm{span}\{\Psi^{\varepsilon}_{n,j,\boldsymbol{k}}(\boldsymbol{x})=2^j\Psi^{\varepsilon}_n(2^j\boldsymbol{x}-\boldsymbol{k})\,,\ \varepsilon,\ j,\boldsymbol{k}\}$ is orthogonal to $\boldsymbol{H}_{\mathrm{div},0}(\mathbb{R}^2)$. We propose a choice for Ψ^{ε}_n, described in appendix B, for which the computation of divergence-free wavelet coefficients $d^{\varepsilon}_{\mathrm{div},j,\boldsymbol{k}}$ is reduced to a very simple linear combination of the standard wavelet coefficients $d^{\varepsilon}_{i,j,\boldsymbol{k}}$.

Now, the expansion (4) of the vector function $\boldsymbol{u}$ can be rewritten

$$\begin{aligned}\boldsymbol{u}=&\sum_{j\in\mathbb{Z}}\sum_{\boldsymbol{k}\in\mathbb{Z}^2}\left(d^{(1,0)}_{\mathrm{div},j,\boldsymbol{k}}\,\Psi^{(1,0)}_{\mathrm{div},j,\boldsymbol{k}}+d^{(0,1)}_{\mathrm{div},j,\boldsymbol{k}}\,\Psi^{(0,1)}_{\mathrm{div},j,\boldsymbol{k}}+d^{(1,1)}_{\mathrm{div},j,\boldsymbol{k}}\,\Psi^{(1,1)}_{\mathrm{div},j,\boldsymbol{k}}\right)\\&+\sum_{j\in\mathbb{Z}}\sum_{\boldsymbol{k}\in\mathbb{Z}^2}\left(d^{(1,0)}_{n,j,\boldsymbol{k}}\,\Psi^{(1,0)}_{n,j,\boldsymbol{k}}+d^{(0,1)}_{n,j,\boldsymbol{k}}\,\Psi^{(0,1)}_{n,j,\boldsymbol{k}}+d^{(1,1)}_{n,j,\boldsymbol{k}}\,\Psi^{(1,1)}_{n,j,\boldsymbol{k}}\right),\end{aligned}\tag{5}$$

where the new coefficients are directly expressed from the original coefficiants by equation (B2) in appendix B. Appendix C summarizes the algorithm in pseudocode. Note that the first line of the above decomposition represents a divergence-free part of $\boldsymbol{u}$, whereas the second line is a complement vector function, not orthogonal to the first.

Remark: $\mathrm{div}(\Psi^{(1,0)}_n)$, $\mathrm{div}(\Psi^{(0,1)}_n)$ and $\mathrm{div}(\Psi^{(1,1)}_n)$ are generating functions of the scalar space $V^0\otimes V^0$. Moreover, we have

$$\mathrm{div}\,\boldsymbol{u}=\sum_{j\in\mathbb{Z}}\sum_{\boldsymbol{k}\in\mathbb{Z}^2}\left[d^{(1,0)}_{n,j,\boldsymbol{k}}\,\mathrm{div}\left(\Psi^{(1,0)}_{n,j,\boldsymbol{k}}\right)+d^{(0,1)}_{n,j,\boldsymbol{k}}\,\mathrm{div}\left(\Psi^{(0,1)}_{n,j,\boldsymbol{k}}\right)+d^{(1,1)}_{n,j,\boldsymbol{k}}\,\mathrm{div}\left(\Psi^{(1,1)}_{n,j,\boldsymbol{k}}\right)\right]$$

Then, the incompressibility condition $\mathrm{div}\,\boldsymbol{u}=0$ is equivalent to $d^{\varepsilon}_{n,j,\boldsymbol{k}}=0$, for all $j,\boldsymbol{k},\varepsilon$.

For incompressible flows, since the biorthogonal projectors onto the spaces $(V^1_j\otimes V^0_j)\times(V^0_j\otimes V^1_j)$ commute with partial derivatives [15], the divergence-free wavelet coefficients $d^{\varepsilon}_{\mathrm{div},j,\boldsymbol{k}}$ are uniquely determined, by the formula (d_{div}) in equation (B2), appendix B. Difficulties arise when we want to compute the divergence-free part of a compressible flow. Because of the non-orthogonality between the divergence-free basis $(\Psi^{\varepsilon}_{\mathrm{div},j,\boldsymbol{k}})$ and its complement $(\Psi^{\varepsilon}_{n,j,\boldsymbol{k}})$, the values of the divergence-free wavelet coefficients depend on the choice of

the complement basis. We address this problem in section 4, in order to provide a wavelet Helmholtz decomposition of any flow. ■

3.1.2 The three-dimensional case. The construction and fast algorithms corresponding to 3D divergence-free wavelet bases are obtained in a similar fashion as for the 2D case, except that one has to start with the following vector MRA of $[L^2(\mathbb{R}^3)]^3$:

$$\left(V_j^1 \otimes V_j^0 \otimes V_j^0\right) \times \left(V_j^0 \otimes V_j^1 \otimes V_j^0\right) \times \left(V_j^0 \otimes V_j^0 \otimes V_j^1\right).$$

From the 21 canonical generating *3D vector wavelets* $\{\Psi_i^\varepsilon \mid i = 1, 2, 3,\ \varepsilon\}$, one constructs 14 generating divergence-free wavelets, and seven complement functions $\Psi_{\mathrm{n}}^\varepsilon$. Appendix B indicates their exact forms (which, for symmetry reasons, differ from the general form (2)). As for the 2D case, the computation of divergence-free wavelet coefficients of any 3D vector field is given by a short linear combination of standard biorthogonal wavelet coefficients, arising from fast wavelet transforms.

3.2 *Anisotropic divergence-free wavelet transforms*

In this section we construct anisotropic wavelets that are divergence free. Since we start from 1D wavelets ψ_0 and ψ_1 verifying $\psi_1{}' = 4\psi_0$, we derive easily divergence-free wavelet bases by tensor products of 1D wavelets. We detail in the following the construction of such bases in the 2D and 3D cases.

3.2.1 The anisotropic two-dimensional case. Unlike the isotropic case, anisotropic divergence-free wavelets are generated from a single vector function

$$\Psi_{\mathrm{div}}^{\mathrm{an}}(x_1, x_2) = \begin{vmatrix} \psi_1(x_1)\psi_0(x_2) \\ -\psi_0(x_1)\psi_1(x_2) \end{vmatrix}$$

by anisotropic dilations, and translations. The 2D anisotropic divergence-free wavelets are given by

$$\Psi_{\mathrm{div},\boldsymbol{j},\boldsymbol{k}}^{\mathrm{an}}(x_1, x_2) = \begin{vmatrix} 2^{j_2}\psi_1(2^{j_1}x_1 - k_1)\psi_0(2^{j_2}x_2 - k_2) \\ -2^{j_1}\psi_0(2^{j_1}x_1 - k_1)\psi_1(2^{j_2}x_2 - k_2) \end{vmatrix},$$

where $\boldsymbol{j} = (j_1, j_2) \in \mathbb{Z}^2$ is the scale parameter, and $\boldsymbol{k} = (k_1, k_2) \in \mathbb{Z}^2$ is the position parameter. When the indices $\boldsymbol{k}$ and $\boldsymbol{j}$ vary in $\mathbb{Z}^2$, the family $\{\Psi_{\mathrm{div},\boldsymbol{j},\boldsymbol{k}}^{\mathrm{an}}\}$ forms a basis of $\boldsymbol{H}_{\mathrm{div},0}(\mathbb{R}^2)$.

We introduced as complement functions:

$$\Psi_{\mathrm{n},\boldsymbol{j},\boldsymbol{k}}^{\mathrm{an}}(x_1, x_2) = \begin{vmatrix} 2^{j_1}\psi_1(2^{j_1}x_1 - k_1)\psi_0(2^{j_2}x_2 - k_2) \\ 2^{j_2}\psi_0(2^{j_1}x_1 - k_1)\psi_1(2^{j_2}x_2 - k_2) \end{vmatrix},$$

since they verify $\Psi_{\mathrm{n},\boldsymbol{j},\boldsymbol{k}}^{\mathrm{an}}$ is orthogonal to $\Psi_{\mathrm{div},\boldsymbol{j},\boldsymbol{k}}^{\mathrm{an}}$ ($\boldsymbol{j}, \boldsymbol{k}$ being fixed).

The anisotropic divergence-free wavelet transform of a given vector function $\boldsymbol{u}$ works similarly to the isotropic transform. Starting from anisotropic wavelet decomposition of $\boldsymbol{u}$ in

the MRA $(V_j^1 \otimes V_j^0) \times (V_j^0 \otimes V_j^1)$ (see appendix A),

$$\boldsymbol{u} = \sum_{\boldsymbol{j}\in\mathbb{Z}^2} \sum_{\boldsymbol{k}\in\mathbb{Z}^2} \left(d^{\text{an}}_{1,\boldsymbol{j},\boldsymbol{k}}\ \Psi^{\text{an}}_{1,\boldsymbol{j},\boldsymbol{k}} + d^{\text{an}}_{2,\boldsymbol{j},\boldsymbol{k}}\ \Psi^{\text{an}}_{2,\boldsymbol{j},\boldsymbol{k}} \right),$$

where

$$\Psi^{\text{an}}_{1,\boldsymbol{j},\boldsymbol{k}}(x_1, x_2) = \begin{vmatrix} \psi_1(2^{j_1}x_1 - k_1)\psi_0(2^{j_2}x_2 - k_2) \\ 0 \end{vmatrix},$$

$$\Psi^{\text{an}}_{2,\boldsymbol{j},\boldsymbol{k}}(x_1, x_2) = \begin{vmatrix} 0 \\ \psi_0(2^{j_1}x_1 - k_1)\psi_1(2^{j_2}x_2 - k_2) \end{vmatrix},$$

for $\boldsymbol{j}, \boldsymbol{k} \in \mathbb{Z}^2$, are the anisotropic canonical wavelets. Note that for more simplicity, the dilated functions are not normalized, in the L^2 norm.

$\boldsymbol{u}$ can be expanded on to the new basis

$$\boldsymbol{u} = \sum_{\boldsymbol{j}\in\mathbb{Z}^2} \sum_{\boldsymbol{k}\in\mathbb{Z}^2} \left(d^{\text{an}}_{\text{div},\boldsymbol{j},\boldsymbol{k}}\ \Psi^{\text{an}}_{\text{div},\boldsymbol{j},\boldsymbol{k}} + d^{\text{an}}_{\text{n},\boldsymbol{j},\boldsymbol{k}}\ \Psi^{\text{an}}_{\text{n},\boldsymbol{j},\boldsymbol{k}} \right), \tag{6}$$

with the corresponding coefficients

$$\begin{aligned} d^{\text{an}}_{\text{div},\boldsymbol{j},\boldsymbol{k}} &= \frac{2^{j_2}}{2^{2j_1} + 2^{2j_2}}\ d^{\text{an}}_{1,\boldsymbol{j},\boldsymbol{k}} - \frac{2^{j_1}}{2^{2j_1} + 2^{2j_2}}\ d^{\text{an}}_{2,\boldsymbol{j},\boldsymbol{k}}, \\ d^{\text{an}}_{\text{n},\boldsymbol{j},\boldsymbol{k}} &= \frac{2^{j_1}}{2^{2j_1} + 2^{2j_2}}\ d^{\text{an}}_{1,\boldsymbol{j},\boldsymbol{k}} + \frac{2^{j_2}}{2^{2j_1} + 2^{2j_2}}\ d^{\text{an}}_{2,\boldsymbol{j},\boldsymbol{k}}, \end{aligned} \tag{7}$$

3.2.2 The anisotropic three-dimensional case. In the same way, the anisotropic 3D divergence-free wavelets take the form

$$\Psi^{\text{an}}_{\text{div},1,\boldsymbol{j},\boldsymbol{k}}(x_1, x_2, x_3) = \begin{vmatrix} 0 \\ 2^{j_3}\psi_0(2^{j_1}x_1 - k_1)\psi_1(2^{j_2}x_2 - k_2)\psi_0(2^{j_3}x_3 - k_3) \\ -2^{j_2}\psi_0(2^{j_1}x_1 - k_1)\psi_0(2^{j_2}x_2 - k_2)\psi_1(2^{j_3}x_3 - k_3) \end{vmatrix},$$

$$\Psi^{\text{an}}_{\text{div},2,\boldsymbol{j},\boldsymbol{k}}(x_1, x_2, x_3) = \begin{vmatrix} -2^{j_3}\psi_1(2^{j_1}x_1 - k_1)\psi_0(2^{j_2}x_2 - k_2)\psi_0(2^{j_3}x_3 - k_3) \\ 0 \\ 2^{j_1}\psi_0(2^{j_1}x_1 - k_1)\psi_0(2^{j_2}x_2 - k_2)\psi_1(2^{j_3}x_3 - k_3) \end{vmatrix},$$

$$\Psi^{\text{an}}_{\text{div},3,\boldsymbol{j},\boldsymbol{k}}(x_1, x_2, x_3) = \begin{vmatrix} 2^{j_2}\psi_1(2^{j_1}x_1 - k_1)\psi_0(2^{j_2}x_2 - k_2)\psi_0(2^{j_3}x_3 - k_3) \\ -2^{j_1}\psi_0(2^{j_1}x_1 - k_1)\psi_1(2^{j_2}x_2 - k_2)\psi_0(2^{j_3}x_3 - k_3) \\ 0 \end{vmatrix},$$

with $\boldsymbol{j} = (j_1, j_2, j_3)$, $\boldsymbol{k} = (k_1, k_2, k_3) \in \mathbb{Z}^3$.

Unlike the 2D case, we have to choose two functions from the three above to generate the divergence-free basis. As complement basis we introduce a function that is most orthogonal to the previous functions:

$$\Psi^{\text{an}}_{\text{n},\boldsymbol{j},\boldsymbol{k}}(x_1, x_2, x_3) = \begin{vmatrix} 2^{j_1}\psi_1(2^{j_1}x_1 - k_1)\psi_0(2^{j_2}x_2 - k_2)\psi_0(2^{j_3}x_3 - k_3) \\ 2^{j_2}\psi_0(2^{j_1}x_1 - k_1)\psi_1(2^{j_2}x_2 - k_2)\psi_0(2^{j_3}x_3 - k_3) \\ 2^{j_3}\psi_0(2^{j_1}x_1 - k_1)\psi_0(2^{j_2}x_2 - k_2)\psi_1(2^{j_3}x_3 - k_3) \end{vmatrix}.$$

The operations to compute divergence-free coefficients and complement coefficients are similar to the 2D case.

4. An iterative algorithm to compute the wavelet Helmholtz decomposition

4.1 *Principle of the Helmholtz decomposition*

The Helmholtz decomposition [27, 28] consists in splitting a vector function $\boldsymbol{u} \in [L^2(\mathrm{R}^n)]^n$ into its divergence-free component $\boldsymbol{u}_{\mathrm{div}}$ and a gradient vector. More precisely, there exist a potential function p and a stream function ψ such that

$$\boldsymbol{u} = \boldsymbol{u}_{\mathrm{div}} + \boldsymbol{\nabla} p \quad \text{and} \quad \boldsymbol{u}_{\mathrm{div}} = \operatorname{curl} \psi. \tag{8}$$

Moreover, the functions curl ψ and $\boldsymbol{\nabla} p$ are orthogonal in $[L^2(\mathbb{R}^n)]^n$. The stream function ψ and the potential function p are unique, up to an additive constant.

In $\mathbb{R}^2$, the stream function is a scalar-valued function, whereas in $\mathbb{R}^3$ it is a 3D vector function. This decomposition may be viewed as the following orthogonal space splitting:

$$[L^2(\mathbb{R}^n)]^n = \boldsymbol{H}_{\mathrm{div},0}(\mathbb{R}^n) \oplus \boldsymbol{H}_{\mathrm{curl},0}(\mathbb{R}^n),$$

where $\boldsymbol{H}_{\mathrm{div},0}(\mathbb{R}^n)$ is the space of divergence-free vector functions, and

$$\boldsymbol{H}_{\mathrm{curl},0}(\mathbb{R}^n) = \{\boldsymbol{v} \in (L^2(\mathbb{R}^n))^n; \quad \operatorname{curl} \boldsymbol{v} \in [L^2(\mathbb{R}^n)]^n, \quad \operatorname{curl} \boldsymbol{v} = \boldsymbol{0}\}$$

is the space of curl-free vector functions (if $n = 2$ we have to replace curl $\boldsymbol{v} \in (L^2(\mathbb{R}^n))^n$ by curl $\boldsymbol{v} \in L^2(\mathbb{R}^2)$ in the definition). For the whole space $\mathbb{R}^n$, the proofs of the above decompositions can be derived easily, by means of the Fourier transform. In more general domains, we refer the reader to [27, 28]. Note that one can also prove that $\boldsymbol{H}_{\mathrm{div},0}(\mathbb{R}^n)$ is the space of curl functions, whereas $\boldsymbol{H}_{\mathrm{curl},0}(\mathbb{R}^n)$ is the space of gradient functions.

The objective now is to generate a wavelet Helmholtz decomposition. Since in the previous sections we have constructed wavelet bases of $\boldsymbol{H}_{\mathrm{div},0}(\mathbb{R}^n)$, we have to work analogously to carry out wavelet bases of $\boldsymbol{H}_{\mathrm{curl},0}(\mathbb{R}^n)$.

4.2 *Construction of a gradient wavelet basis*

A definition of wavelet bases for the space $\boldsymbol{H}_{\mathrm{curl},0}(\mathbb{R}^n)$ ($n = 2, 3$) has already been provided by Urban [22] in the isotropic case. We shall focus here on the construction of *anisotropic* curl-free vector wavelets in the 2D case (it is similar in the n-dimensional case).

This construction is very similar to the divergence-free wavelet construction, despite some crucial differences. The starting point here is to search wavelets in the MRA $(V_j^0 \otimes V_j^1) \times (V_j^1 \otimes V_j^0)$ instead of $(V_j^1 \otimes V_j^0) \times (V_j^0 \otimes V_j^1)$, where the 1D spaces V_0 and V_1 are related by differentiation and integration (section 2.1).

Since $\boldsymbol{H}_{\mathrm{curl},0}(\mathbb{R}^2)$ is the space of gradient functions in $L^2(\mathbb{R}^2)$, we construct gradient wavelets by taking the gradient of a 2D wavelet basis of the MRA $(V_j^1 \otimes V_j^1)$. If we neglect the L^2 normalization, the anisotropic gradient wavelets are defined by

$$\Psi^{\mathrm{an}}_{\mathrm{curl},\boldsymbol{j},\boldsymbol{k}}(x_1, x_2) = \frac{1}{4} \boldsymbol{\nabla}[\psi_1(2^{j_1}x_1 - k_1)\psi_1(2^{j_2}x_2 - k_2)] = \begin{vmatrix} 2^{j_1}\psi_0(2^{j_1}x_1 - k_1)\psi_1(2^{j_2}x_2 - k_2) \\ 2^{j_2}\psi_1(2^{j_1}x_1 - k_1)\psi_0(2^{j_2}x_2 - k_2) \end{vmatrix}.$$

Thus, when $\boldsymbol{j} = (j_1, j_2)$, $\boldsymbol{k} = (k_1, k_2)$ vary in $\mathbb{Z}^2$, the family $\{\Psi^{\mathrm{an}}_{\mathrm{curl},\boldsymbol{j},\boldsymbol{k}}\}$ forms a wavelet basis of $\boldsymbol{H}_{\mathrm{curl},0}(\mathbb{R}^2)$.

The decomposition algorithm on curl-free wavelets $\{\Psi^{\text{an}}_{\text{curl},\boldsymbol{j},\boldsymbol{k}}\}$ works similarly to that on anisotropic divergence-free wavelets. Starting from the anisotropic wavelet decomposition of a vector function $\boldsymbol{v}$ in the MRA $(V_j^0 \otimes V_j^1) \times (V_j^1 \otimes V_j^0)$,

$$\boldsymbol{v} = \sum_{\boldsymbol{j}\in\mathbb{Z}^2} \sum_{\boldsymbol{k}\in\mathbb{Z}^2} \left(d^{\text{an}}_{1,\boldsymbol{j},\boldsymbol{k}}\ \Psi^{\text{an},\#}_{1,\boldsymbol{j},\boldsymbol{k}} + d^{\text{an}}_{2,\boldsymbol{j},\boldsymbol{k}}\ \Psi^{\text{an},\#}_{2,\boldsymbol{j},\boldsymbol{k}}\right),$$

where the canonical anisotropic vector wavelets are

$$\Psi^{\text{an},\#}_{1,\boldsymbol{j},\boldsymbol{k}}(x_1,x_2) = \begin{vmatrix} \psi_0(2^{j_1}x_1 - k_1)\psi_1(2^{j_2}x_2 - k_2), \\ 0 \end{vmatrix}$$

$$\Psi^{\text{an},\#}_{2,\boldsymbol{j},\boldsymbol{k}}(x_1,x_2) = \begin{vmatrix} 0 \\ \psi_1(2^{j_1}x_1 - k_1)\psi_0(2^{j_2}x_2 - k_2). \end{vmatrix}$$

By applying the change in basis

$$\begin{cases} \Psi^{\text{an},\#}_{1,\boldsymbol{j},\boldsymbol{k}} \\ \Psi^{\text{an},\#}_{2,\boldsymbol{j},\boldsymbol{k}} \end{cases} \longrightarrow \begin{cases} \Psi^{\text{an}}_{\text{curl},\boldsymbol{j},\boldsymbol{k}} = 2^{j_1}\Psi^{\text{an},\#}_{1,\boldsymbol{j},\boldsymbol{k}} + 2^{j_2}\Psi^{\text{an},\#}_{2,\boldsymbol{j},\boldsymbol{k}}, \\ \Psi^{\text{an}}_{N,\boldsymbol{j},\boldsymbol{k}} \ = 2^{j_2}\Psi^{\text{an},\#}_{1,\boldsymbol{j},\boldsymbol{k}} - 2^{j_1}\Psi^{\text{an},\#}_{2,\boldsymbol{j},\boldsymbol{k}}, \end{cases}$$

we obtain

$$\boldsymbol{v} = \sum_{\boldsymbol{j}\in\mathbb{Z}^2} \sum_{\boldsymbol{k}\in\mathbb{Z}^2} \left(d^{\text{an}}_{\text{curl},\boldsymbol{j},\boldsymbol{k}}\ \Psi^{\text{an}}_{\text{curl},\boldsymbol{j},\boldsymbol{k}} + d^{\text{an}}_{N,\boldsymbol{j},\boldsymbol{k}}\Psi^{\text{an}}_{N,\boldsymbol{j},\boldsymbol{k}}\right), \tag{9}$$

where the curl-free wavelet coefficients are obtained from the standard coefficients by

$$d^{\text{an}}_{\text{curl},\boldsymbol{j},\boldsymbol{k}} = \frac{2^{j_1}}{2^{2j_1}+2^{2j_2}}\ d^{\text{an}}_{1,\boldsymbol{j},\boldsymbol{k}} + \frac{2^{j_2}}{2^{2j_1}+2^{2j_2}}\ d^{\text{an}}_{2,\boldsymbol{j},\boldsymbol{k}} \tag{10}$$

and have associated complement coefficients

$$d^{\text{an}}_{N,\boldsymbol{j},\boldsymbol{k}} = \frac{2^{j_2}}{2^{2j_1}+2^{2j_2}}\ d^{\text{an}}_{1,\boldsymbol{j},\boldsymbol{k}} - \frac{2^{j_1}}{2^{2j_1}+2^{2j_2}}\ d^{\text{an}}_{2,\boldsymbol{j},\boldsymbol{k}}. \tag{11}$$

4.3 *Implementation of the Helmholtz decomposition in the wavelet context*

From now on, our objective is to compute the wavelet decomposition of a given vector function $\boldsymbol{v}$; this means that we want to find a divergence-free component $\boldsymbol{v}_{\text{div}}$ and an orthogonal curl-free component $\boldsymbol{v}_{\text{curl}}$ such that

$$\boldsymbol{v} = \boldsymbol{v}_{\text{div}} + \boldsymbol{v}_{\text{curl}},$$

where

$$\boldsymbol{v}_{\text{div}} = \sum_{\boldsymbol{j},\boldsymbol{k}} d_{\text{div},\boldsymbol{j},\boldsymbol{k}}\Psi_{\text{div},\boldsymbol{j},\boldsymbol{k}}, \quad \mathbf{v}_{\text{curl}} = \sum_{\boldsymbol{j},\boldsymbol{k}} d_{\text{curl},\boldsymbol{j},\boldsymbol{k}}\Psi_{\text{curl},\boldsymbol{j},\boldsymbol{k}},$$

are the wavelet expansions on to divergence-free and curl-free wavelet bases constructed previously (sections 3.2.1 and 4.2). We shall focus here on 2D anisotropic wavelet bases (and we shall omit the superscript an in the notation of the basis functions).

To provide such decomposition, we have to overcome two problems.

First, the divergence-free wavelets and curl-free wavelets form *biorthogonal* bases in their respective spaces and, as already noticed by Urban [22], they do not give rise, in a simple way, to the orthogonal projections $\boldsymbol{v}_{\text{div}}$ and $\boldsymbol{v}_{\text{curl}}$ of $\boldsymbol{v}$. As a solution, we propose to construct, in wavelet spaces, two sequences $(\boldsymbol{v}^p_{\text{div}})$ and $(\boldsymbol{v}^p_{\text{curl}})$ that converge to $\boldsymbol{v}_{\text{div}}$ and $\boldsymbol{v}_{\text{curl}}$.

The second difficulty is that divergence-free wavelets are in spaces of the form $(V_J^1 \otimes V_J^0) \times (V_J^0 \otimes V_J^1)$, whereas curl-free wavelets are in $(\tilde{V}_J^0 \otimes \tilde{V}_J^1) \times (\tilde{V}_J^1 \otimes \tilde{V}_J^0)$, where V_0^0, V_0^1 and $\tilde{V}_0^0$, $\tilde{V}_0^1$ are couples of spaces related by differentiation and integration. These spaces are different, and in order to construct our approximations $(\boldsymbol{v}_{\text{div}}^p)$ and $(\boldsymbol{v}_{\text{curl}}^p)$, we have to define a precise interpolation procedure between them. In particular, the spaces $\tilde{V}_0^0$, $\tilde{V}_0^1$ can be suitably chosen from V_0^0, V_0^1.

4.3.1 Iterative construction of the divergence-free and curl-free parts of a flow. Let $\boldsymbol{v} = (v_1, v_2)$ be a vector function, and suppose that $\boldsymbol{v}$ is periodic in both directions and known on $2^J \times 2^J$ grid points that are not necessarily the same for v_1 and v_2. In the following, we denote by $\mathbb{I}_J \boldsymbol{v}$ an approximation of $\boldsymbol{v}$ in the space $(V_J^1 \otimes V_J^0) \times (V_J^0 \otimes V_J^1)$, given by some interpolation process, and by $\mathbb{I}_J^{\#} \boldsymbol{v}$ an approximation of $\boldsymbol{v}$ in the space $(\tilde{V}_J^0 \otimes \tilde{V}_J^1) \times (\tilde{V}_J^1 \otimes \tilde{V}_J^0)$, also given by some interpolation process.

We now define the sequences $\boldsymbol{v}_{\text{div}}^p \in (V_J^1 \otimes V_J^0) \times (V_J^0 \otimes V_J^1)$ satisfying $\operatorname{div} \boldsymbol{v}_{\text{div}}^p = 0$, and $\boldsymbol{v}_{\text{curl}}^p \in (\tilde{V}_J^0 \otimes \tilde{V}_J^1) \times (\tilde{V}_J^1 \otimes \tilde{V}_J^0)$ satisfying $\operatorname{curl} \boldsymbol{v}_{\text{curl}}^p = 0$, as follows.

We begin with $\boldsymbol{v}^0 = \mathbb{I}_J \boldsymbol{v}$, and we compute $\boldsymbol{v}_{\text{div}}^0$, the divergence-free wavelet decomposition of $\boldsymbol{v}^0$, and its complement $\boldsymbol{v}_{\text{n}}^0$, by formula from equations (6) and (7):

$$\mathbb{I}_J \boldsymbol{v} = \boldsymbol{v}_{\text{div}}^0 + \boldsymbol{v}_{\text{n}}^0 = \sum_{\boldsymbol{j},\boldsymbol{k}} d_{\text{div},\boldsymbol{j},\boldsymbol{k}}^0 \, \Psi_{\text{div},\boldsymbol{j},\boldsymbol{k}} + \sum_{\boldsymbol{j},\boldsymbol{k}} d_{\text{n},\boldsymbol{j},\boldsymbol{k}}^0 \, \Psi_{\text{n},\boldsymbol{j},\boldsymbol{k}}.$$

Then we compute the difference $\boldsymbol{v} - \boldsymbol{v}_{\text{div}}^0$ at collocation points.

Secondly we consider $\mathbb{I}_J^{\#}(\boldsymbol{v} - \boldsymbol{v}_{\text{div}}^0)$, and we apply the curl-free wavelet decomposition (9)–(11), leading to a curl-free part and its complement:

$$\mathbb{I}_J^{\#}(\boldsymbol{v} - \boldsymbol{v}_{\text{div}}^0) = \boldsymbol{v}_{\text{curl}}^0 + \boldsymbol{v}_N^0 = \sum_{\boldsymbol{j},\boldsymbol{k}} d_{\text{curl},\boldsymbol{j},\boldsymbol{k}}^0 \, \Psi_{\text{curl},\boldsymbol{j},\boldsymbol{k}} + \sum_{\boldsymbol{j},\boldsymbol{k}} d_{\text{N},\boldsymbol{j},\boldsymbol{k}}^0 \Psi_{\text{N},\boldsymbol{j},\boldsymbol{k}}.$$

Finally we define $\boldsymbol{v}^1$ *pointwise* by $\boldsymbol{v}^1 = \boldsymbol{v} - \boldsymbol{v}_{\text{div}}^0 - \boldsymbol{v}_{\text{curl}}^0$.

At step p, by knowing $\boldsymbol{v}^p$ at grid points, we are able to construct a divergence-free part $\boldsymbol{v}_{\text{div}}^p$ of $\mathbb{I}_J \boldsymbol{v}^p$ from equation (6), and $\boldsymbol{v}_{\text{curl}}^p$, the curl-free component of $\mathbb{I}_J^{\#}(\boldsymbol{v}^p - \boldsymbol{v}_{\text{div}}^p)$ from equation (9) ($\boldsymbol{v}^p - \boldsymbol{v}_{\text{div}}^p$ being computed at grid points). The next term of the sequence is again defined pointwise:

$$\boldsymbol{v}^{p+1} = \boldsymbol{v}^p - \boldsymbol{v}_{\text{div}}^p - \boldsymbol{v}_{\text{curl}}^p. \tag{12}$$

We iterate this process until $\|\boldsymbol{v}^P\|_{\ell^2} < \epsilon$, and we obtain

$$\begin{aligned} \boldsymbol{v} &\approx_\epsilon \sum_{p=1}^{P} \boldsymbol{v}_{\text{div}}^p + \sum_{p=1}^{P} \boldsymbol{v}_{\text{curl}}^p \\ &= \sum_{\boldsymbol{j},\boldsymbol{k}} \left(\sum_{p=1}^{P} d_{\text{div},\boldsymbol{j},\boldsymbol{k}}^p \right) \Psi_{\text{div},\boldsymbol{j},\boldsymbol{k}} + \sum_{\boldsymbol{j},\boldsymbol{k}} \left(\sum_{p=1}^{P} d_{\text{curl},\boldsymbol{j},\boldsymbol{k}}^p \right) \Psi_{\text{curl},\boldsymbol{j},\boldsymbol{k}}, \end{aligned}$$

where the right-hand side is an approximation of $\boldsymbol{v}$, which interpolates the data up to an error ϵ (ϵ being given).

Ideally, the iteration converges as indicated on figure 3. However, we are not able to prove the convergence of the sequence $(\boldsymbol{v}^p)$. We shall demonstrate it experimentally in section 6.4, on arbitrary fields. Nevertheless, we outline some remarks.

The convergence rate depends on the choice of complement functions $\Psi_{n,\boldsymbol{j},\boldsymbol{k}}$, $\Psi_{N,\boldsymbol{j},\boldsymbol{k}}$. The smaller the L^2 scalar products $\langle \Psi_{\text{div},\boldsymbol{j},\boldsymbol{k}} | \Psi_{n,\boldsymbol{j}',\boldsymbol{k}'} \rangle$ and $\langle \Psi_{\text{curl},\boldsymbol{j},\boldsymbol{k}} | \Psi_{N,\boldsymbol{j}',\boldsymbol{k}'} \rangle$, the faster the sequences converge.

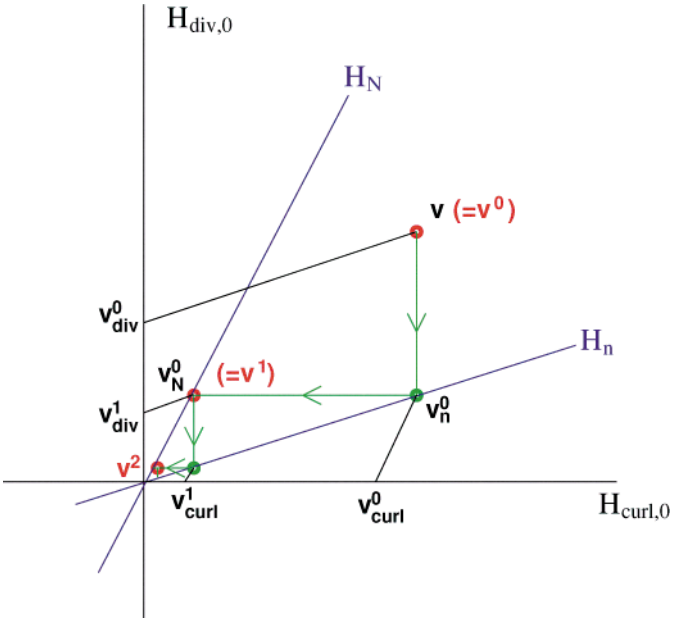

Figure 3. Idealistic schematization of the convergence process of the algorithm with $H_N = \text{span}\{\Psi_{N,j,k}\}$ and $H_n = \text{span}\{\Psi_{n,j,k}\}$.

Ideally, we would like the convergence rate to be independent of the interpolating operators $\mathbb{I}_J$ and $\mathbb{I}_J^{\#}$. We propose below a choice for these operators, based on spline quasi-interpolation, which is satisfactory at relatively slow convergence rate.

4.3.2 Helmholtz-adapted spline interpolation. In this section, we shall detail our choice of operators $\mathbb{I}_J$ and $\mathbb{I}_J^{\#}$, in the context of the spline spaces of degree 1 (V_j^0) and degree 2 (V_j^1) that we introduced earlier.

Let us suppose that the components v_1 and v_2 of a velocity field $\boldsymbol{v}$ are known at knot points $2^{-J}(k_1 + \frac{1}{2}, k_2)$ and $2^{-J}(k_1, k_2 + \frac{1}{2})$ respectively, for $k_1, k_2 = 0, 2^J - 1$. This choice of grid is induced by the symmetry centres of scaling functions ϕ_0 of V_0^0 and ϕ_1 of V_0^1 (figure 4).

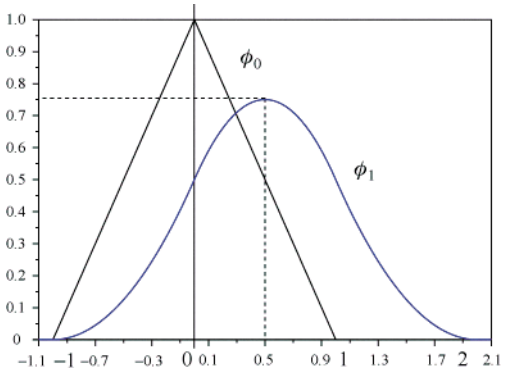

Figure 4. The two scaling functions of V_0^0 and V_0^1, and their symmetry centres.

For J given, $\mathbb{I}_J$ is chosen as a quasi-interpolation operator (similarly to section 6.1.2) in the spline space $(V_J^1 \otimes V_J^0) \times (V_J^0 \otimes V_J^1)$:

$$\mathbb{I}_J \boldsymbol{v} = \sum_{\boldsymbol{k}} c_{\boldsymbol{k}}^1 \, \Phi_{1,J,\boldsymbol{k}} + \sum_{\boldsymbol{k}} c_{\boldsymbol{k}}^2 \, \Phi_{2,J,\boldsymbol{k}},$$

where Φ_1 and Φ_2 are the vector scaling functions introduced in section 3.1.1.

The second operator $\mathbb{I}_J^{\#}$ provides a quasi-interpolation of vector functions on to a new spline space $(\tilde{V}_J^0 \otimes \tilde{V}_J^1) \times (\tilde{V}_J^1 \otimes \tilde{V}_J^0)$. Under interpolation considerations, we define

$$\tilde{V}_0^0 = \left\{ \boldsymbol{v} \; ; \; \boldsymbol{v}(x - 1/2) \in V_0^0 \right\} = \text{span}\{\phi_0(x - 1/2 - k) \; ; \; k \in \mathbb{Z}\},$$

$$\tilde{V}_0^1 = \left\{ \boldsymbol{v} \; ; \; \boldsymbol{v}(x - 1/2) \in V_0^1 \right\} = \text{span}\{\phi_1(x - 1/2 - k) \; ; \; k \in \mathbb{Z}\},$$

Hence we can write

$$\mathbb{I}_J^{\#} \boldsymbol{v} = \sum_{\boldsymbol{k}} c_{\boldsymbol{k}}^{\#1} \, \tilde{\Phi}_{1,J,\boldsymbol{k}} + \sum_{\boldsymbol{k}} c_{\boldsymbol{k}}^{\#2} \, \tilde{\Phi}_{2,J,\boldsymbol{k}},$$

where $\tilde{\Phi}_{1,J,\boldsymbol{k}}$ and $\tilde{\Phi}_{2,J,\boldsymbol{k}}$ are the 2D vector scaling functions of the MRA $(\tilde{V}_J^0 \otimes \tilde{V}_J^1) \times (\tilde{V}_J^1 \otimes \tilde{V}_J^0)$.

5. A divergence-free wavelet method for the Navier–Stokes equations

We present in this section the basics of a divergence-free wavelet numerical method, for the resolution of the incompressible Navier–Stokes equations, written in velocity–pressure formulation (without forcing term) as

$$\begin{cases} \dfrac{\partial \boldsymbol{u}}{\partial t} + (\boldsymbol{u} \cdot \boldsymbol{\nabla})\boldsymbol{u} + \boldsymbol{\nabla} p - \nu \Delta \boldsymbol{u} = 0, \\ \boldsymbol{\nabla}.\boldsymbol{u} = 0, \end{cases} \tag{13}$$

with periodic or Dirichlet boundary conditions, in a square (or cubic) domain.

Our objective is to derive a Galerkin method based on finite-dimensional spaces of divergence-free wavelets. Galerkin (or Petrov–Galerkin) methods are variational methods for DNS of turbulence. In the context of wavelet Galerkin or Petrov–Galerkin methods (including collocation methods), in [4–7], numerical methods were proposed for the resolution of the 2D Navier–Stokes equations in *vorticity–stream function* formulation, with periodic boundary conditions. However, these methods cannot extend in a simple way to the 3D case nor to Dirichlet boundary conditions. In the $(\boldsymbol{u}, p)$ formulation with classical discretizations, like spectral methods (in the non-periodic case) [29], finite-element methods [27], or (non-divergence-free) wavelets [9, 11], one has to adapt the discretization bases for velocity and pressure, in order to satisfy some inf–sup condition (also called 9, 11 condition), or one has to introduce some stabilization term to avoid spurious modes in the computation of the pressure. Then system (13) leads to a saddle-point problem. Depending on the chosen formulation (Galerkin, collocation, etc.) this problem is usually solved by the Uzawa algorithm, or by a splitting method. In any case, numerical difficulties arise in the computation of the pressure, which requires solution of the ill-conditioned linear system of Schur complement, or a Poisson equation.

When using divergence-free bases, this difficulty is totally avoided; indeed, the pressure disappears by projecting the first of equations of (13) on to the divergence-free vector functions:

$$\frac{\partial \boldsymbol{u}}{\partial t} + \mathbb{P}[(\boldsymbol{u} \cdot \boldsymbol{\nabla})\boldsymbol{u}] - \nu \Delta \boldsymbol{u} = 0, \tag{14}$$

where $\mathbb{P}$ denotes the Leray projector. The solution $\boldsymbol{u}$ then has the form

$$\boldsymbol{u}(\boldsymbol{x}, t) = \sum_{\boldsymbol{j},\boldsymbol{k}} u_{\mathrm{div},\boldsymbol{j},\boldsymbol{k}}(t)\ \Psi_{\mathrm{div},\boldsymbol{j},\boldsymbol{k}}(\boldsymbol{x}).$$

After projecting equation (14) onto a finite dimensional wavelet subspace

$$\mathrm{span}\{\Psi_{\mathrm{div},(j_1,j_2),\boldsymbol{k}}\ ;\ j_1, j_2 < J\},$$

Equation (14) is simply reduced to a system of ordinary differential equations, which can be solved by a classical finite-difference or Runge–Kutta scheme. The main difficulty in this approach is the computation of $\mathbb{P}[(\boldsymbol{u}\cdot\boldsymbol{\nabla})\boldsymbol{u}]$. However, the Helmholtz decomposition of the nonlinear term yields

$$(\boldsymbol{u}.\boldsymbol{\nabla})\boldsymbol{u} = \mathbb{P}[(\boldsymbol{u}.\boldsymbol{\nabla})\boldsymbol{u}] - \boldsymbol{\nabla} p,$$

where p is the flow pressure.

The wavelet Helmoltz decomposition presented in section 4 allows us to write

$$\begin{aligned}(\boldsymbol{u}.\boldsymbol{\nabla})\boldsymbol{u} &= \mathbb{P}[(\boldsymbol{u}.\boldsymbol{\nabla})\boldsymbol{u}] + [(\boldsymbol{u}.\boldsymbol{\nabla})\boldsymbol{u}]_{\mathrm{curl}} \\ &= \sum_{\boldsymbol{j},\boldsymbol{k}} d_{\mathrm{div},\boldsymbol{j},\boldsymbol{k}}(t)\ \Psi_{\mathrm{div},\boldsymbol{j},\boldsymbol{k}}(\boldsymbol{x}) + \sum_{\boldsymbol{j},\boldsymbol{k}} d_{\mathrm{curl},\boldsymbol{j},\boldsymbol{k}}(t)\ \Psi_{\mathrm{curl},\boldsymbol{j},\boldsymbol{k}}(\boldsymbol{x}).\end{aligned}$$

Then we get the divergence-free wavelet decomposition of $\mathbb{P}[(\boldsymbol{u}.\boldsymbol{\nabla})\boldsymbol{u}] = \sum_{\boldsymbol{j},\boldsymbol{k}} d_{\mathrm{div},\boldsymbol{j},\boldsymbol{k}}(t)\ \Psi_{\mathrm{div},\boldsymbol{j},\boldsymbol{k}}(\boldsymbol{x})$. The second term gives the pressure from the curl-free coefficients of $\boldsymbol{\nabla} p$ as follows.

5.1 *Computation of the pressure*

Remember that curl-free wavelets are constructed by

$$\Psi^{\mathrm{an}}_{\mathrm{curl},\boldsymbol{j},\boldsymbol{k}}(\boldsymbol{x}) = \frac{1}{4}\,\boldsymbol{\nabla}[\psi_1(2^{j_1}x_1 - k_1)\psi_1(2^{j_2}x_2 - k_2)], \quad \boldsymbol{j} = (j_1, j_2), \quad \boldsymbol{k} = (k_1, k_2).$$

From the equalities

$$\begin{aligned}-\boldsymbol{\nabla} p &= [(\boldsymbol{u}.\boldsymbol{\nabla})\boldsymbol{u}]_{\mathrm{curl}} \\ &= \sum_{\boldsymbol{j},\boldsymbol{k}} d_{\mathrm{curl},\boldsymbol{j},\boldsymbol{k}}(t)\ \Psi_{\mathrm{curl},\boldsymbol{j},\boldsymbol{k}}(\boldsymbol{x}) \\ &= \sum_{\boldsymbol{j},\boldsymbol{k}} d_{\mathrm{curl},\boldsymbol{j},\boldsymbol{k}}(t)\ \frac{1}{4}\,\boldsymbol{\nabla}[\psi_1(2^{j_1}x_1 - k_1)\psi_1(2^{j_2}x_2 - k_2)],\end{aligned}$$

one directly obtains by integration

$$-4p = \sum_{\boldsymbol{j},\boldsymbol{k}} d_{\mathrm{curl},\boldsymbol{j},\boldsymbol{k}}(t)\ \psi_1(2^{j_1}x_1 - k_1)\psi_1(2^{j_2}x_2 - k_2).$$

Thus the computation of the pressure is no more than a standard anisotropic wavelet reconstruction in $V_j^1 \otimes V_j^1$, from the curl-free coefficients of the nonlinear term obtained through the wavelet Helmoltz decomposition.

6. Numerical experiments

In this section we present the numerical results of the application of the divergence-free wavelet decomposition. We begin with the analysis of periodic numerical incompressible velocity fields in two and three dimensions, generated by pseudospectral codes. First, we have to take care of the initial interpolation of such fields, in order not to violate the incompressibility condition satisfied in Fourier space. Then, after the vizualization of the divergence-free wavelet coefficients, we shall study the compression factor obtained through the wavelet decomposition. Finally, we investigate and numerically demonstrate the convergence of the algorithm presented in section 4.3, which provides the wavelet Helmholtz decomposition of any flow. In order to validate the approach that we proposed in section 5, we compute, in wavelet space, the divergence-free component of a nonlinear term of the Navier-Stokes equations, and we extract the associated pressure. In all the experiments, we use divergence-free wavelets constructed with splines of degree 1 and degree 2.

6.1 *Approximation of the velocity in spline spaces*

Usually, the velocity fields are given by grid point values. The first step of the wavelet decomposition consists in interpolating these velocity data on a suitable B-spline space. The problem is that this approximation may not conserve the divergence-free condition, a condition that was satisfied in Fourier space when velocity data come from a spectral code.

The spline approximation of data, obtained through spectral methods, introduces a slight error for the divergence-free condition. This difference may be not negligible. For the turbulent fields that we studied (2D and 3D) the error is about 1% of the L^2 norm of the velocity.

Thus we propose two ways to overcome this problem. The first way is to interpolate the velocity in the Fourier domain and to compute exactly its biorthogonal projection on wavelet spaces. The second way is to interpolate on the divergence-free B-spline spaces with the wavelet Helmholtz decomposition detailed in section 4.3.1.

6.1.1 By using the discrete Fourier transform. Since they are highly accurate, spectral methods are often considered as a reference technique for simulating incompressible turbulent flows. For periodic boundary conditions on the cube $[0, 1]^2$, the discrete Fourier transform (DFT) is used to decompose the velocity $\boldsymbol{u}$.

If $\hat{\boldsymbol{u}}_{\boldsymbol{k}}$ means the (vector) discrete Fourier coefficients of $\boldsymbol{u}$ on a N^2 regular grid given by

$$\hat{\boldsymbol{u}}_{\boldsymbol{k}} = \frac{1}{N^2} \sum_{\boldsymbol{n}\in\{0,1,\ldots,N-1\}^2} \boldsymbol{u}\left(\frac{\boldsymbol{n}}{N}\right) e^{-2i\pi \boldsymbol{k}\cdot\boldsymbol{n}/N},$$

the velocity expansion in the Fourier exponential basis is

$$\boldsymbol{u}(\boldsymbol{x}) = \sum_{\boldsymbol{k}\in\{0,1,\ldots,N-1\}^2} \hat{\boldsymbol{u}}_{\boldsymbol{k}}\, e^{2i\pi \boldsymbol{k}\cdot\boldsymbol{x}}. \tag{15}$$

In this context, the divergence-free condition $\operatorname{div} \boldsymbol{u} = 0$ is

$$\boldsymbol{k}\cdot\hat{\boldsymbol{u}}_{\boldsymbol{k}} = 0, \quad \forall \boldsymbol{k} \in \{0, 1, \ldots, N-1\}^2. \tag{16}$$

Assume now that the velocity field $\boldsymbol{u}$ to be analysed (assumed to be 1-periodic in both directions), comes from a spectral method and satisfies the incompressibility condition in the Fourier domain (16). To compute its decomposition in a divergence-free wavelet basis of $\mathbb{R}^2$, we have first to approximate $\boldsymbol{u} = (u_1, u_2)$ in the suitable space $(V_J^1 \otimes V_J^0) \times (V_J^0$

$\otimes\, V_J^1$) introduced in section 3.1.1, where J corresponds to $N = 2^J$. Then we search for an approximate function $\boldsymbol{u}_J = (u_{J\,1}, u_{J\,2})$ such that

$$\boldsymbol{u}_{J\,1} = \sum_{n_1=0}^{2^J-1}\sum_{n_2=0}^{2^J-1} c^1_{J,n_1,n_2}\,\phi_{1,J,n_1}\phi_{0,J,n_2},$$

$$\boldsymbol{u}_{J\,2} = \sum_{n_1=0}^{2^J-1}\sum_{n_2=0}^{2^J-1} c^2_{J,n_1,n_2}\,\phi_{0,J,n_1}\phi_{1,J,n_2}.$$

For the choice of functions ϕ_0 and ϕ_1 verifying equation (1), the incompressibility condition $\operatorname{div} \boldsymbol{u}_J = 0$ takes the discrete form on the coefficients c^i_{J,n_1,n_2}:

$$c^1_{J,n_1,n_2} - c^1_{J,n_1+1,n_2} + c^2_{J,n_1,n_2} - c^2_{J,n_1,n_2+1} = 0, \quad \forall (n_1, n_2). \tag{17}$$

To conserve the incompressibility condition satisfied by $\boldsymbol{u}$, a solution consists in considering $\boldsymbol{u}_J$ as the biorthogonal projection on to the space $(V_J^1 \otimes V_J^0) \times (V_J^0 \otimes V_J^1)$, since we know that this projector commutes with partial derivatives [15]. This is equivalent to considering that

$$c^1_{J,n_1,n_2} = \langle \boldsymbol{u} \mid \phi^*_{1,J,n_1}\phi^*_{0,J,n_2}\rangle,$$
$$c^2_{J,n_1,n_2} = \langle \boldsymbol{u} \mid \phi^*_{0,J,n_1}\phi^*_{1,J,n_2}\rangle.$$

Replacing $\boldsymbol{u}$ by its Fourier expansion (15), it follows that

$$\begin{aligned} c^1_{J,n_1,n_2} &= \sum_{\boldsymbol{k}\in\{0,1,\ldots,N-1\}^2} \hat{\boldsymbol{u}}_{\boldsymbol{k}} \iint_{\mathbb{R}^2} e^{2i\pi \boldsymbol{k}\cdot\boldsymbol{x}}\, \phi^*_{1,J,n_1}(x_1)\,\phi^*_{0,J,n_2}(x_2)\;\mathrm{d}x_1\mathrm{d}x_2 \\ &= 2^{-J} \sum_{\boldsymbol{k}\in\{0,1,\ldots,N-1\}^2} \hat{\boldsymbol{u}}_{\boldsymbol{k}}\, \overline{\hat{\phi}^*_1(2^{-J}2\pi k_1)}\;\; \overline{\hat{\phi}^*_0(2^{-J}2\pi k_2)}\;\, \mathrm{e}^{2i\pi \boldsymbol{k}\cdot\boldsymbol{n}/2^J}, \end{aligned}$$

where $\hat{\phi}^*_1, \hat{\phi}^*_2$ denote the (continuous) Fourier transforms of the dual scaling functions ϕ^*_1, ϕ^*_2. Finally, we obtain an explicit form for the DFT of the coefficients c^1_{J,n_1,n_2} (and in the same way for c^2_{J,n_1,n_2}):

$$\begin{aligned} \mathrm{DFT}\big(c^1_{J,\boldsymbol{n}}\big)_{\boldsymbol{k}} &= \hat{\boldsymbol{u}}_{\boldsymbol{k}}\, 2^{-J}\, \overline{\hat{\phi}^*_1(2^{-J}(2\pi k_1))}\;\, \overline{\hat{\phi}^*_0(2^{-J}(2\pi k_2))}, \\ \mathrm{DFT}\big(c^2_{J,\boldsymbol{n}}\big)_{\boldsymbol{k}} &= \hat{\boldsymbol{u}}_{\boldsymbol{k}}\, 2^{-J}\, \overline{\hat{\phi}^*_0(2^{-J}(2\pi k_1))}\;\, \overline{\hat{\phi}^*_1(2^{-J}(2\pi k_2))}. \end{aligned} \tag{18}$$

This means that the DFT of coefficients c^i_{J,n_1,n_2} is given by the DFT of $\boldsymbol{u}$, multiplied by tabulated values on $[0, 2\pi]$ of the Fourier transform of the duals $\hat{\phi}^*_1, \hat{\phi}^*_2$. In practice, we do not know the explicit forms of these functions, except by the infinite product:

$$\hat{\phi}^*_0(\xi) = \hat{\phi}_0(\xi)\,\Pi_{j>1}[2-\cos(\xi 2^{-j})] \;= \left(\frac{\sin(\xi/2)}{\xi/2}\right)^2 \Pi_{j>1}[2-\cos(\xi 2^{-j})],$$

$$\hat{\phi}^*_1(\xi) = \hat{\phi}^*_0\,(\xi)\left(\frac{e^{i\xi}-1}{i\xi}\right) \;=\; e^{i\xi/2} \quad \hat{\phi}^*_0(\xi)\left(\frac{\sin(\xi/2)}{\xi/2}\right),$$

Nevertheless, the infinite product converges rapidly, which allows us to obtain point values of $\hat{\phi}^*_0$ and $\hat{\phi}^*_1$, with sufficient accuracy.

In three dimensions, one proceeds similarly, by considering the biorthogonal projection of a 3D vector field $\boldsymbol{u}$ on to the space $(V_J^1 \otimes V_J^0 \otimes V_J^0) \times (V_J^0 \otimes V_J^1 \otimes V_J^0) \times (V_J^0 \otimes V_J^0 \otimes V_J^1)$.

6.1.2 By quasi-interpolation. The spline quasi-interpolation is a good compromise when we have to deal simultaneously with spline approximations of even and odd degrees. In this context, the order of approximation is $n+1$, by using B splines of degree n [30]. An advantage of the procedure is that it may be applied for any boundary conditions.

Let b be a B-spline scaling function ($b = \phi_0$ or ϕ_1). Given the sampling $f(k/N)$ ($N = 2^J$), we want to compute scaling coefficients c_k, of a spline function f_N, that will nearly interpolate the values $f(k/N)$:

$$f_N(x) = \sum_{k\in\mathbb{Z}} c_k\, b(Nx - k). \tag{19}$$

f_N is an interpolating function if

$$\sum_{k\in\mathbb{Z}} c_k\, b(\ell - k) = f\left(\frac{\ell}{N}\right) \quad \forall \ell \in \mathbb{Z}.$$

For example, if we consider $b = \phi_1$ (spline of degree 2), the previous condition implies that

$$f_N\left(\frac{\ell}{N}\right) = \frac{1}{2}\,(c_{\ell-1} + c_\ell) = f\left(\frac{\ell}{N}\right) \quad \forall \ell \in \mathbb{Z}.$$

In order to avoid the inversion of a linear system, the quasi-interpolation introduces, instead of c_ℓ,

$$\widetilde{c}_\ell = \frac{5}{8}\left[f\left(\frac{\ell}{N}\right) + f\left(\frac{\ell+1}{N}\right)\right] - \frac{1}{8}\left[f\left(\frac{\ell-1}{N}\right) + f\left(\frac{\ell+2}{N}\right)\right] \quad \forall \ell \in \mathbb{Z}.$$

By replacing c_ℓ by $\widetilde{c}_\ell$ in equation (19), we obtain the following error at each grid point:

$$\begin{aligned} 1/2\big(\widetilde{c}_{\ell-1} + \widetilde{c}_\ell\big) - f\left(\frac{\ell}{N}\right) &= \frac{1}{16}\Bigg[- f\left(\frac{\ell-2}{N}\right) \\ &\quad + 4f\left(\frac{\ell-1}{N}\right) - 6f\left(\frac{\ell}{N}\right) + 4f\left(\frac{\ell+1}{N}\right) - f\left(\frac{\ell+2}{N}\right)\Bigg] \\ &= -\frac{1}{48N^4} f^{(4)}(\theta) + O\left(\frac{1}{N^6}\right), \\ &\quad \text{with} \quad \theta \in \left[\frac{\ell-2}{N}, \frac{\ell+2}{N}\right] \end{aligned}$$

Therefore, the pointwise error of quasi-interpolation is of order 4, for a sufficiently regular function.

6.2 *Analysis of two-dimensional incompressible fields*

We focus in this section on the analysis of 2D decaying turbulent flows.

The first numerical experiment that we present analyses the merging of two same-sign vortices. It concerns free decaying turbulence (no forcing term). The experiment was originally designed by Schneider *et al.* [7] and has often been used to test new numerical methods [4, 9]. The experiment of [4] was reproduced here by using a pseudospectral method, solving the Navier–Stokes equations in a velocity–pressure formulation.

The initial state is displayed in figure 5, left. In a periodic box, three vortices with a Gaussian vorticity profile are present; two are positive with the same intensity, and one is negative with half the intensity of the others. The negative vortex is here to force the merging of the two

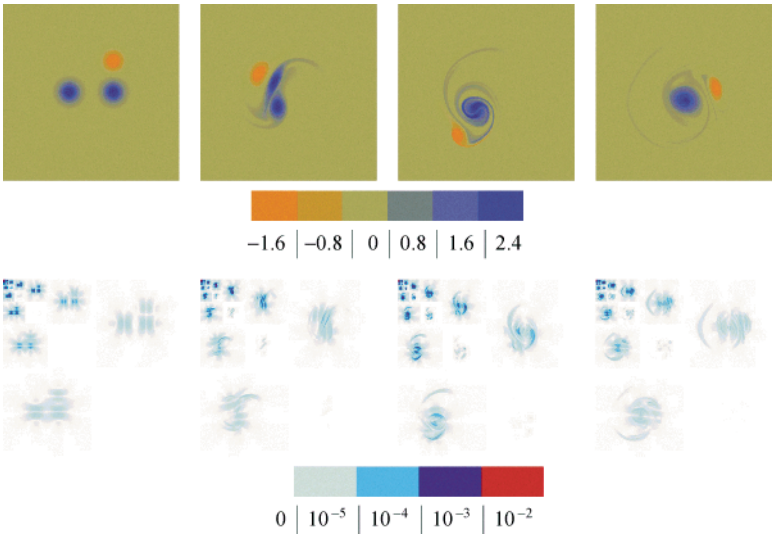

Figure 5. Vorticity fields at times $t = 0$, $t = 10$, $t = 20$ and $t = 40$, and corresponding divergence-free wavelet coefficients of the velocity.

positive vortices. The time step was $\delta t = 10^{-2}$ and the viscosity $\nu = 5 \times 10^{-5}$. The solution is computed on a 512×512 grid.

The vorticity fields at times $t = 0, t = 10, t = 20$ and $t = 40$ are displayed in figure 5. The second row of figure 5 displays the absolute values of the isotropic divergence-free wavelet coefficients of the *velocity field* at corresponding times, renormalized by 2^j at scale index j. As one can see, divergence-free wavelet coefficients concentrate on strong energy zones, which correspond to a region of strong variations in the velocity, that is around or in between vortices, or along vorticity filaments.

The second experiment deals with a decaying 2D turbulent field, obtained with an initial state of the random phase spectrum. This vorticity field was computed with a spectral code at a resolution 1024×1024 (see [31] for more details). As noticed in [31], there is a Newtonian viscosity such that the Reynolds number is 3.5×10^4. This field has been kindly provided to us by Lapeyre [32] and was published in [31]. After 40 turnover timescales of the predominant eddies, for a timescale based upon the total enstrophy of the flow, the vorticity field exhibits the emergence of coherent structures together with strong filamentation of the flow field outside the vortices (figure 6, left).

We show, in figure 7, the isotropic and anisotropic divergence-free wavelet coefficients (in the $L^{\inf}$ -norm) issued from the decomposition of the velocity field displayed in figure 6 (right). We must emphasize that, before computing the divergence-free wavelet coefficients, we first had to compute the velocity field from the vorticity field (this is done in the Fourier domain).

As expected, the wavelet coefficients give insight into the energy distribution over the scales of the flow. As one can see in figure 7 (left), the energy on the smallest scale (or highest wave numbers) is localized along the strong deformation lines and fits the filamentation between vortices, or with strong changes in vortices. The top right square corresponding to vertical isotropic wavelets ($\Psi^{(1,0)}_{\mathrm{div},j,\boldsymbol{k}}$) exhibits vertical structures, whereas the bottom left square corresponding to horizontal wavelets ($\Psi^{(0,1)}_{\mathrm{div},j,\boldsymbol{k}}$) exhibits horizontal deformation lines.

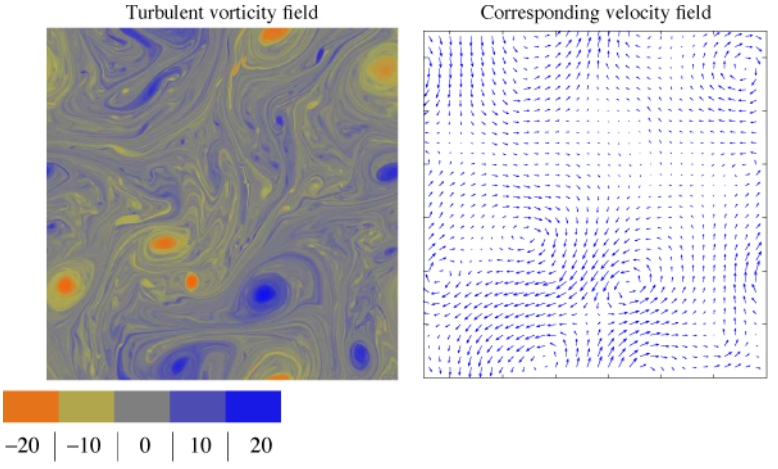

Figure 6. Vorticity field for a 1024×1024 simulation of decaying turbulence (left), and the corresponding velocity field (right).

Now we investigate the compression properties of the divergence-free wavelet analysis: as predicted by the nonlinear approximation theory [26]; the compression ratio in the energy norm is governed by the underlying regularity of the velocity field in some Besov space.

Let $\boldsymbol{u}$ be an incompressible field, its divergence-free wavelet expansion can be written

$$\boldsymbol{u} = \boldsymbol{u}_0 + \sum_{j \geq 0} \sum_{\boldsymbol{k} \in \mathbb{Z}^2} \left(d^{(1,0)}_{\mathrm{div},j,\boldsymbol{k}} \, \Psi^{(1,0)}_{\mathrm{div},j,\boldsymbol{k}} + d^{(0,1)}_{\mathrm{div},j,\boldsymbol{k}} \, \Psi^{(0,1)}_{\mathrm{div},j,\boldsymbol{k}} + d^{(1,1)}_{\mathrm{div},j,\boldsymbol{k}} \, \Psi^{(1,1)}_{\mathrm{div},j,\boldsymbol{k}} \right).$$

The nonlinear approximation of $\boldsymbol{u}$ relies on computing the best N-term wavelet approximation by reordering the wavelet coefficients

$$\left| d^{\varepsilon_1}_{\mathrm{div},j_1,\boldsymbol{k}_1} \right| > \left| d^{\varepsilon_2}_{\mathrm{div},j_2,\boldsymbol{k}_2} \right| > \cdots > \left| d^{\varepsilon_N}_{\mathrm{div},j_N,\boldsymbol{k}_N} \right| > \cdots$$

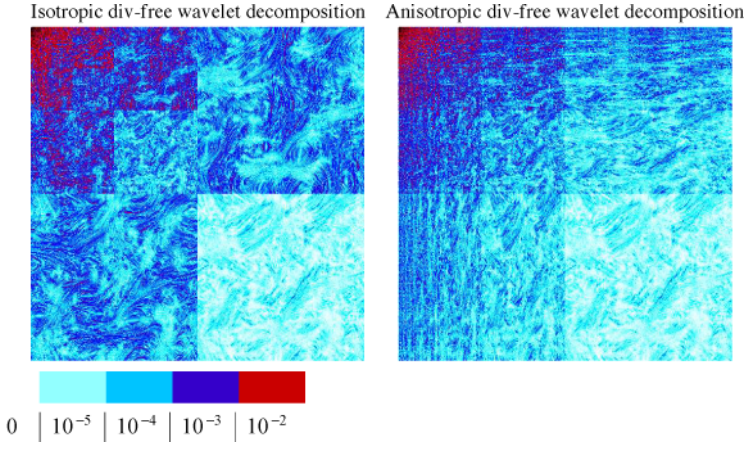

Figure 7. Isotropic (left) and anisotropic (right) divergence-free wavelet coefficients of the velocity field of figure 6 (right).

and introducing

$$\Sigma_N(\boldsymbol{u}) = \boldsymbol{u}_0 + \sum_{i=1}^{N} d^{\varepsilon_i}_{\mathrm{div},j_i,\boldsymbol{k}_i}\ \Psi^{\varepsilon_i}_{\mathrm{div},j_i,\boldsymbol{k}_i}. \tag{20}$$

Then we have

$$\|\boldsymbol{u} - \Sigma_N(\boldsymbol{u})\|_{L^2} < C\left(\frac{1}{N}\right)^{s/n} \|\boldsymbol{u}\|_{B^{s,q}_q} \tag{21}$$

if the quantity $\|\boldsymbol{u}\|^q_{B^{s,q}_q} = \sum_{\varepsilon,j,\boldsymbol{k}} |d^{\varepsilon}_{\mathrm{div},j,\boldsymbol{k}}|^q$ is finite, with $1/q = 1/2 + s/n$ (this means that $\boldsymbol{u}$ belongs to the Besov space $B^{s,q}_q$). As stated in [26], the evaluated regularity s cannot be larger than the order of polynomial reproduction in scaling spaces plus one (which equals the number of zero moments of the dual wavelet). In our experiment, the dual spline wavelets ψ^*_0 and ψ^*_1 (see appendix A) have respectively two and three zero moments, which allows us to evaluate regularities only smaller than two.

Figure 8 shows the nonlinear compression of divergence-free wavelets, provided on the 1024^2 turbulent field. The curve represents the L^2 error $\|\boldsymbol{u} - \Sigma_N(\boldsymbol{u})\|_{L^2}$ versus N in a log–log plot. The convergence rate measured on the curve is s ($= 2\ p$ with p the slope of the curve) $\approx$1.35, which shows that the velocity flow belongs to the corresponding Besov space $B^{s,q}_q$ with $q = 0.85$.

When looking at the compression curve on figure 8, we observe three different zones.

First, large-scale wavelets capture large-scale structures of the flows. Consequently, the compression progresses slowly and irregularly.

Then we observe a linear slope that represents the nonlinear structure of the turbulent flows. In this region, we are able to evaluate the regularity of the field.

The last region corresponds to an abrupt decrease, because the data are discrete.

One can also remark that, in figure 8, only 1.2% of the coefficients recover about 99% of the L^2-norm.

The same experiment was carried out on the three interacting vortices but is not reported here, since the slope of the curves saturates at $s = 2$, because of the small number of vanishing moments of the wavelets we use (equal to 2 in our experiment); this means that these fields are more regular and suggests using wavelets with more vanishing moments to optimize the compression factor.

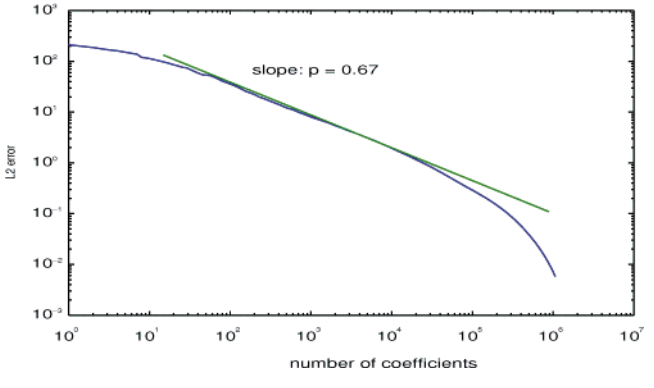

Figure 8. L^2 error provided by the nonlinear N best terms of the wavelet approximation (20); the log–log plot shows the L^2 error (21) versus N for a 2D turbulent flow.

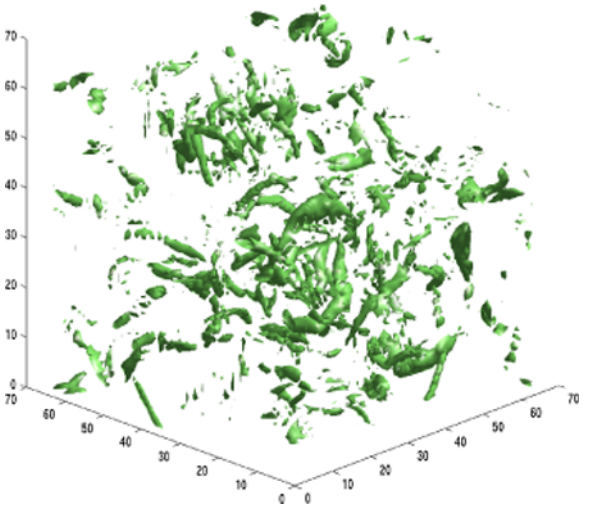

Figure 9. Isosurface 12.45 of vorticity magnitude after five large-eddy turnovers provided by a spectral method [33].

6.3 *Analysis of a three-dimensional incompressible field*

In this part we consider a 3D periodic field, generated from DNS (spectral method) of freely decaying isotropic turbulence, kindly provided to us by G.-H. Cottet and B. Michaux. The experiment has been detailed in [33] and was a Gaussian initial condition for the velocity and 128^3 collocation points. Figure 9 displays the vorticity isosurfaces corresponding to about 40% of the maximum vorticity at five turnover times (time being expressed in terms of large-eddy turnover time units L_0/u_0, where L_0 is the initial integral scale and $\boldsymbol{u}_0^2 = 2/3\boldsymbol{u}(0)^2$). The Reynold number based on the Taylor microscale is initially 98 and decreases to 26 at $t = 8$ (see [33] for more details).

The isotropic divergence-free wavelet decomposition of the corresponding *velocity* field is computed, and displayed in figures 10 and 11. As explained in section 3.1.2, the isotropic 3D divergence-free wavelet decomposition provides 14 generating wavelets $\Psi^{\varepsilon}_{\mathrm{div},1,j,\boldsymbol{k}}$, $\Psi^{\varepsilon}_{\mathrm{div},2,j,\boldsymbol{k}}$.

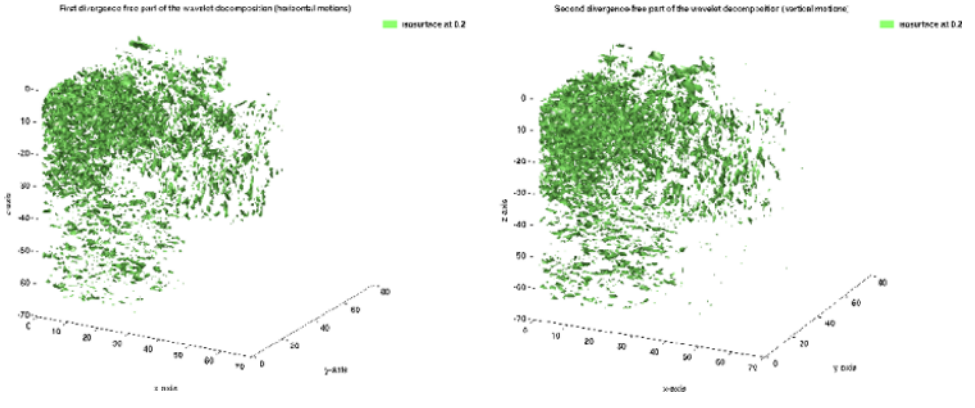

Figure 10. Isosurface 0.2 of divergence-free wavelet coefficients associated with $\Psi^{\varepsilon}_{\mathrm{div},1,j,\boldsymbol{k}}$ (left) and to $\Psi^{\varepsilon}_{\mathrm{div},2,j,\boldsymbol{k}}$ (right), in absolute value.

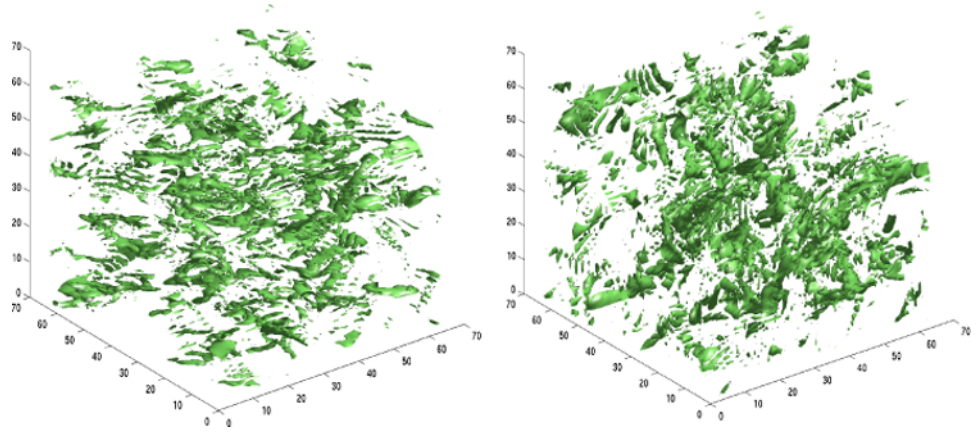

Figure 11. Isosurface 0.06 of divergence-free wavelet coefficients associated with $\Psi^{(1,0,0)}_{\mathrm{div},2,j,\boldsymbol{k}}$ (left) and to $\Psi^{(0,0,1)}_{\mathrm{div},1,j,\boldsymbol{k}}$ (right), in absolute value.

Figure 10, left, shows the corresponding renormalized coefficients $2^j d_{\mathrm{div},1,j,\boldsymbol{k}}$, whereas figure 10, right, shows $2^j d_{\mathrm{div},2,j,\boldsymbol{k}}$, up to $j = 6$. The smallest scale ($j = 7$) wavelet coefficients are displayed in figure 11, for two different generating wavelets; we choose $\Psi^{(1,0,0)}_{\mathrm{div},2}$, which corresponds to horizontal structures, and $\Psi^{(0,0,1)}_{\mathrm{div},1}$ which exhibits vertical structures.

Figure 12 displays the nonlinear compression error: unlike the 2D case, owing to the low resolution (128^3 instead of 1024^2) of the field, it is difficult to detect a linear part in the curve. Nethertheless, in an intermediate region, the curve nearly presents a slope of $s\ (= 3\ p) \approx 1.45$.

6.4 *Wavelet Helmholtz decomposition of velocity fields*

6.4.1 Convergence of the method. The wavelet Helmholtz decomposition presented in section 4. is tested in order to demonstrate numerically that our algorithm converges. In this part, we apply the method of section 4.3 to random 2D vector fields $\boldsymbol{v}$ (defined as mathematical functions, whithout physical meaning), and we study the behaviour of the residual $\|\boldsymbol{v}^P\|_{\ell^2}$ (see section 4.3). These vector fields are constructed with a uniform random law at each collocation

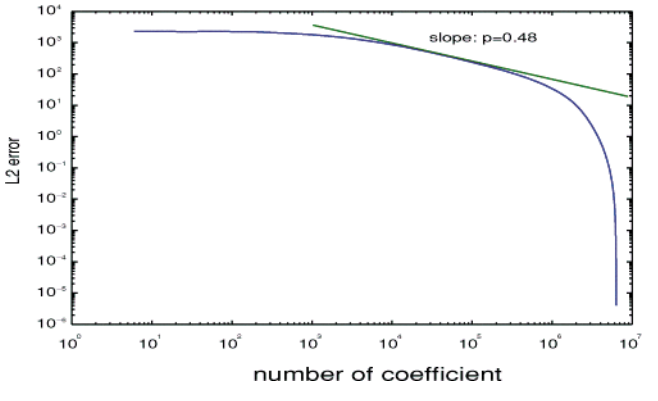

Figure 12. L^2 error provided by the nonlinear N best terms of the wavelet approximation (20); the log-log plot, shows the L^2 error (21) versus N for a 3D turbulent flow.

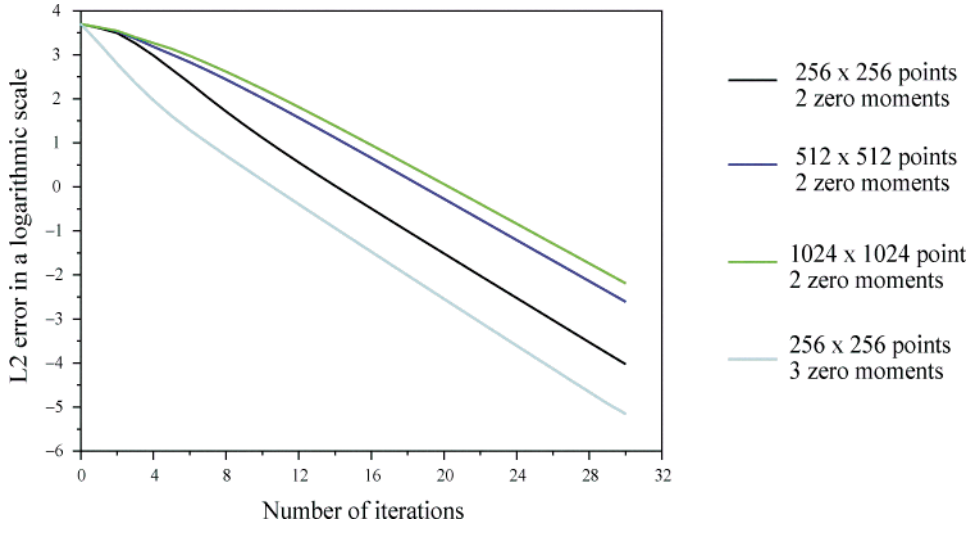

Figure 13. Convergence curves of the iterative wavelet Helmholtz algorithm.

point. Figure 13 displays the ℓ^2 norm of the residual $\|\boldsymbol{v}^P\|_{\ell^2}$, in terms of the number of iterations p, in four different situations (different sizes for $\boldsymbol{v}$; different zero moments for the wavelets). We make the following conclusions.

(i) For all functions that we have tested, the method converges, and the curves show that, except at the very beginning, the convergence is exponential.
(ii) The slope of the curve hardly depends on the number of grid points (it is steeper with fewer grid points).
(iii) The convergence rate increases with increasing number of vanishing moments of the dual wavelets.

Now, if we want to estimate the numerical cost of the wavelet Leray projection (divergence-free part) of a given (compressible) vector field, we have to compare it with the cost of the Leray projection in the Fourier domain, namely $\mathrm{O}(N \log_2 N)$, if N is the number of grid points. Since the price to pay for a fast wavelet transform is $\mathrm{O}(N)$ operations, and since in numerical experiments the wavelet Helmholtz algorithm converges in about 20 iterations to reach an error of 10^{-6}, the whole cost is $\mathrm{O}(20N)$ which is asymptotically better.

In the future, we shall investigate the influence of the wavelet bases and of the interpolation projectors on the convergence rate.

6.4.2 Wavelet Helmholtz decomposition of the nonlinear term of the Navier–Stokes equations. Since our main objective for further research is to use divergence-free wavelets to solve numerically the Navier–Stokes equations (see section 5), we have to find the wavelet–Helmholtz decomposition of the nonlinear term $(\boldsymbol{u} \cdot \boldsymbol{\nabla})\boldsymbol{u}$. To illustrate the feasibility of our approach, we consider the 2D turbulent field displayed in figure 6, and we compute the divergence-free and curl-free wavelet components of its associated nonlinear term $(\boldsymbol{u} \cdot \boldsymbol{\nabla})\boldsymbol{u}$ using the wavelet Helmholtz decomposition; figure 14 shows the anisotropic wavelet coefficients (L^∞ normalized) of the divergence-free part (left) and of the curl-free part (right) arising from this decomposition. The wavelet coefficients are displayed as indicated in figure A2 of appendix A. One can see the appearance of small-scale wavelet coefficients (at the bottom

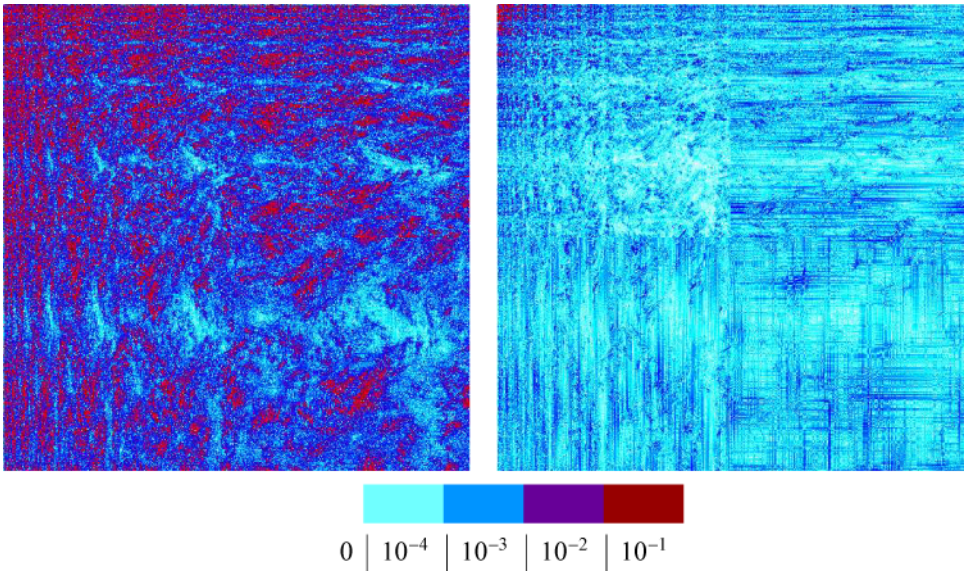

Figure 14. Anisotropic wavelet coefficients corresponding to the wavelet Helmholtz decomposition of $(\boldsymbol{u} \cdot \nabla)\boldsymbol{u}$: divergence-free coefficients (left), and curl-free coefficients (right).

right of each square of wavelet decomposition) in the decomposition of the divergence-free part, by comparison with the decomposition in figure 7; it is obvious that the nonlinear term contributes to the creation of small scales.

From the divergence-free wavelet coefficients in figure 14, we reconstruct the divergence-free part of $(\boldsymbol{u} \cdot \nabla)\boldsymbol{u}$ and display in figure 15 (left) the vorticity field associated with this

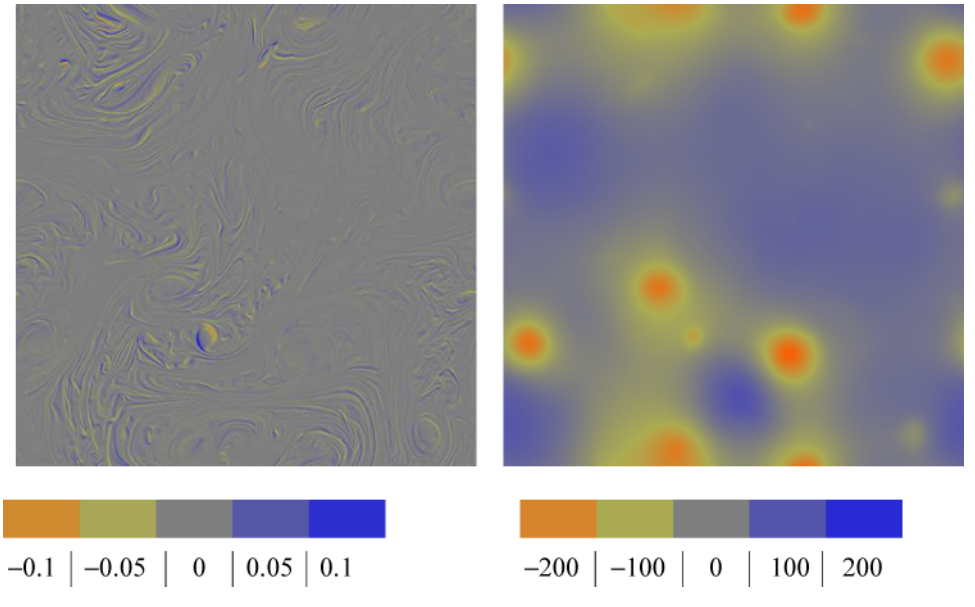

Figure 15. Vorticity (left) and differential pressure (right) derived from the wavelet Helmholtz decomposition of the nonlinear term $(\boldsymbol{u} \cdot \nabla)\boldsymbol{u}$, with $\boldsymbol{u}$ displayed in figure 6.

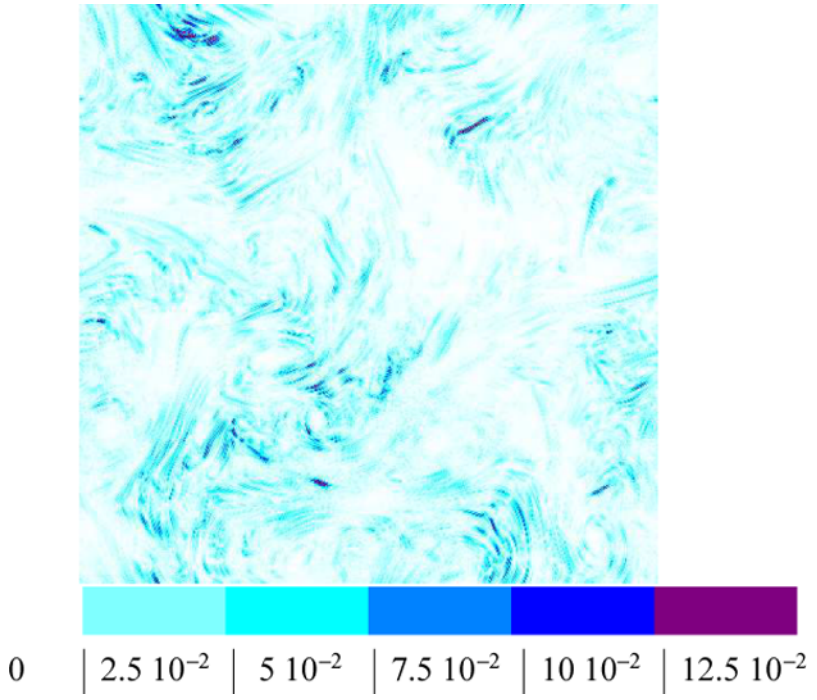

Figure 16. Relative error between the divergence-free part of $(\boldsymbol{u} \cdot \boldsymbol{\nabla})\boldsymbol{u}$ (obtained through Fourier transform) and the part provided by the wavelet Helmholtz decomposition.

velocity. This visualization confirms the creation of small-scale structures in the nonlinear term. Figure 15 (right) displays the reconstruction of the pressure, from curl-free wavelet coefficients, as explained in section 5. As expected, low pressures correspond to coherent vortices.

To control our results, we have compared the pressure obtained by the wavelet Helmoltz decomposition to that computed in the Fourier domain, and we have found a relative error of 2.5×10^{-4} in the L^2 norm, an error which probably arose from the interpolation procedure. On the other hand, the difference between the Leray projection (in Fourier space) and the wavelet projection on to the divergence-free space represents 1% of the L^2 norm. Figure 16 displays the localization of this error. As one can see, the error is localized around strong gradients of the field, which are zones where the Fourier interpolation and the spline interpolation (preliminary step before projecting in both cases) do not give the same result.

7. Conclusion and perspectives

We have presented in detail the construction of 2D and 3D divergence-free wavelet bases, and a practical way to compute their associated coefficients. We have introduced *anisotropic* divergence-free and curl-free wavelet bases, which are easier to handle. We have shown that these bases make possible an iterative algorithm to compute the wavelet Helmholtz decomposition of any flow. Thus, numerical tests prove the feasibility of divergence-free wavelets for simulating turbulent flows in two dimensions and three dimensions. A divergence-free wavelet-based solver for 2D Navier-Stokes equations in $(\boldsymbol{u}, p)$ formulation is under way and will be reported in a forthcoming paper.

An important issue that must be addressed is the flexibility of the method; although all numerical tests have been presented in the periodic case, the method extends readily to non-periodic problems in square or cubic domains by using wavelets incorporating homogeneous boundary conditions such as those in [34, 35]. Indeed, the construction of divergence-free wavelets with non-periodic boundary conditions has already been carried on by Urban [22]. Another point is that, since we consider the $(\boldsymbol{u}, p)$ formulation for the Navier–Stokes equation, and since we are able to compute the Leray projector in the wavelet domain, the method extends easily to the 3D case. Finally, we conjecture that this method should be competitive with finite-element methods and spectral methods in the *non-periodic* case, since in this case classical methods involve a saddle-point problem, and since wavelet methods take advantage of the compression properties of the wavelet bases both for functions and for operators (in the periodic case, the comparison would be unfair, since the spectral methods are clearly optimal).

Appendix A: Multiresolution analysis

A.1 *Introduction*

MRAs are approximation spaces allowing the construction of wavelet bases and were introduced by Mallat [25]. We recall here some definitions.

Definition: A multiresolution analysis (MRA) of $L^2(\mathbb{R})$ is a sequence of closed subspaces $(V_j)_{j\in\mathbb{Z}}$ verifying the following.

(i) $\forall j, V_j \subset V_{j+1}, \quad \bigcap_{j\in\mathbb{Z}} V_j = \{0\}, \quad \bigcup_{j\in\mathbb{Z}} V_j$ is dense in $L^2(\mathbb{R})$.
(ii) (Dilation invariance) $\quad f \in V_j \quad \Longleftrightarrow \quad f(2.) \in V_{j+1}$.
(iii) (Shift invariance) There exists a function $\phi \in V_0$ such that $V_0 = \text{span}\,\{\phi(\cdot - k); k \in \mathbb{Z}\}$.

ϕ is called a *scaling function* of the MRA. j denotes the level of refinement. By virtue of equation (ii), one has $V_j = \text{span}\,\{\phi_{j,k}(x) = 2^{j/2}\phi(2^j x - k); k \in \mathbb{Z}\}$.

Wavelets appear as bases of complementary spaces W_j such that $V_{j+1} = V_j \oplus W_j$, where the sum is direct, but not necessarily orthogonal. In this context (called the biorthogonal case introduced in [36]), the choice of spaces W_j is not unique. In each space W_j, one can construct a function ψ, called a *wavelet* such that $W_j = \text{span}\{\psi_{j,k} = 2^{j/2}\psi(2^j \cdot -k); k \in \mathbb{Z}\}$. Then the wavelet space decomposition of $L^2(\mathbb{R})$ is written

$$L^2(\mathbb{R}) = V_0 \bigoplus_{j=0}^{+\infty} W_j$$

and any function $f \in L^2(\mathbb{R})$ has the following wavelet expansion:

$$f(x) = \sum_{k\in\mathbb{Z}} c_k \phi(x-k) + \sum_{j>0}\sum_{k\in\mathbb{Z}} d_{j,k}\psi_{j,k}(x). \tag{A1}$$

A.2 *Biorthogonal basis*

As (ϕ, ψ) is fixed, we can associate a unique dual pair (ϕ^*, ψ^*), such that the following biorthogonality (in space L^2) relations are fulfilled: $\forall k \in \mathbb{Z}$ and $\forall j > 0$,

$$\langle \phi | \phi_k^* \rangle = \delta_{k,0}, \quad \langle \phi | \psi_{j,k}^* \rangle = 0, \quad \langle \psi | \psi_{j,k}^* \rangle = \delta_{j,0}\delta_{k,0}, \quad \langle \psi | \phi_k^* \rangle = 0,$$

where $\phi_k^* = \phi^*(\cdot - k)$ and $\psi_{j,k}^* = 2^{j/2}\psi^*(2^j \cdot - k)$. In equation (A1), the scaling coefficients c_k and the wavelet coefficients $d_{j,k}$ can be obtained by

$$c_k = \langle f|\phi_k^*\rangle, \quad d_{j,k} = \langle f|\psi_{j,k}^*\rangle.$$

A.3 *Scaling equations and filter design*

Since the function $(1/2^{1/2})\phi(\cdot/2)$ lives in V_0, there exists a sequence (h_k) (also called the *low-pass filter*), verifying that

$$\frac{1}{2^{1/2}}\phi\left(\frac{x}{2}\right) = \sum_{k\in\mathbb{Z}} h_k\, \phi(x-k). \tag{A2}$$

By applying the Fourier transform†, equation (A2) can be rewritten

$$\hat{\phi}(2\xi) = m_0(\xi)\hat{\phi}(\xi),$$

where $m_0(\xi) = (1/2^{1/2})\sum_{k\in\mathbb{Z}} h_k e^{-ik\xi}$ is the transfer function of the filter (h_k).

Again, because $W_{-1} \subset V_0$, the wavelet satisfies a two-scale equation

$$\frac{1}{2^{1/2}}\psi\left(\frac{x}{2}\right) = \sum_{k\in\mathbb{Z}} g_k\, \phi(x-k), \tag{A3}$$

where the coefficients (g_k) are called the *high-pass filter*. Again the Fourier transform of ψ is expressed with the transfer function n_0 of filter g_k as

$$\hat{\psi}(2\xi) = n_0(\xi)\hat{\phi}(\xi).$$

In the same way, the dual functions satisfy the scaling equations

$$\begin{aligned}
&\frac{1}{2^{1/2}}\phi^*\left(\frac{x}{2}\right) = \sum_{k\in\mathbb{Z}} h_k^*\, \phi^*(x-k), \quad \hat{\phi}^*(2\xi) = m_0^*(\xi)\hat{\phi}^*(\xi),\\
&\frac{1}{2^{1/2}}\psi^*\left(\frac{x}{2}\right) = \sum_{k\in\mathbb{Z}} g_k^*\, \phi^*(x-k), \quad \hat{\psi}^*(2\xi) = n_0^*(\xi)\hat{\phi}^*(\xi),
\end{aligned} \tag{A4}$$

And the relations between the transfer functions are

$$n_0(\xi) = \mathrm{e}^{-\mathrm{i}\xi}\,\overline{m_0^*(\xi+\pi)}, \quad n_0^*(\xi) = \mathrm{e}^{-\mathrm{i}\xi}\,\overline{m_0(\xi+\pi)},$$

which corresponds to

$$g_k = (-1)^{1-k}\, h_{1-k}^*, \quad g_k^* = (-1)^{1-k}\, h_{1-k}, \quad \forall k.$$

In practice, the filter coefficients h_k and g_k are all that is needed to compute the wavelet decomposition (A1) of a given function. Note that these filters are finite if and only if the functions ψ and ϕ are compactly supported. Fast wavelet algorithms provide the computation of $N = 2^J$ wavelet coefficients with $\mathrm{O}(2^J)$ operation when the filters are finite [25].

Example: symmetric biorthogonal splines of degree 1: A simple example for spaces V_j are the spaces of continuous functions, which are piecewise linear on the intervals $[k2^{-j}, (k+1)2^{-j}]$, for $k \in \mathbb{Z}$. In this case we can choose as scaling function the hat function

†The Fourier transform of a function f is defined by $\hat{f}(\xi) = \int_{-\infty}^{+\infty} f(x)\,\mathrm{e}^{\mathrm{i}x\xi}\,\alpha x$,

Table C1. Decomposition filter $(h_k^*,\ g_k^*)$ and reconstruction filter $(h_k,\ g_k)$ coefficients, associated with piecewise linear splines (left) and piecewise quadratic splines (right), verifying derivation conditions (1) with the shortest supports.

ℓ	-2	-1	0	1	2	3
$\frac{1}{2^{1/2}}h_\ell^{*0}$	$\frac{-1}{8}$	$\frac{1}{4}$	$\frac{3}{4}$	$\frac{1}{4}$	$\frac{-1}{8}$	0
$\frac{1}{2^{1/2}}g_\ell^{*0}$	0	0	$\frac{-1}{4}$	$\frac{1}{2}$	$\frac{-1}{4}$	0
$\frac{1}{2^{1/2}}h_\ell^{0}$	0	$\frac{1}{4}$	$\frac{1}{2}$	$\frac{1}{4}$	0	0
$\frac{1}{2^{1/2}}g_\ell^{0}$	0	$\frac{-1}{8}$	$\frac{-1}{4}$	$\frac{3}{4}$	$\frac{-1}{4}$	$\frac{-1}{8}$
$2^{1/2}h_\ell^{*1}$		$\frac{-1}{4}$	$\frac{3}{4}$	$\frac{3}{4}$	$\frac{-1}{4}$	
$2^{1/2}g_\ell^{*1}$		$\frac{1}{8}$	$\frac{-3}{8}$	$\frac{3}{8}$	$\frac{-1}{8}$	
$\frac{1}{2^{1/2}}h_l^{1}$		$\frac{1}{8}$	$\frac{3}{8}$	$\frac{3}{8}$	$\frac{1}{8}$	
$\frac{1}{2^{1/2}}g_l^{1}$		$\frac{-1}{4}$	$\frac{-3}{4}$	$\frac{3}{4}$	$\frac{1}{4}$	

$\phi(x) = \max(0, 1 - |x|)$. Its transfer function is given by

$$m_0(\xi) = \mathrm{e}^{\mathrm{i}\xi}\left(\frac{1+\mathrm{e}^{-\mathrm{i}\xi}}{2}\right)^2. \tag{A5}$$

The shortest even dual scaling function associated with ϕ is associated with the filter

$$m_0^*(\xi) = \mathrm{e}^{\mathrm{i}\xi}\left(\frac{1+\mathrm{e}^{-\mathrm{i}\xi}}{2}\right)^2(2-\cos\xi). \tag{A6}$$

The corresponding values of filters (h_k) and (h_k^*) are given in table 1, appendix C. Figure A1 displays the scaling functions and their associated wavelets in this case.

A.4 *Multivariate wavelets*

The above considerations can be extended to multidimensions. The simplest way to obtain multivariate wavelets is to use anisotropic or isotropic tensor products of 1D functions.

The anisotropic 2D wavelets are constructed with tensor products of wavelets of different scales $\{\Psi_{\boldsymbol{j},\boldsymbol{k}}^{an}(x, y) = \psi_{j_1,k_1}(x)\tilde{\psi}_{j_2,k_2}(y);\ \boldsymbol{j} = (j_1, j_2) \in \mathbb{Z}^2,\ \boldsymbol{k} = (k_1, k_2) \in \mathbb{Z}^2\}$, where $\psi_{j,k}$ and $\tilde{\psi}_{j,k}$ are 1D wavelet bases. Note that these bases can come from different MRAs (V_j and $\tilde{V}_j$).

The anisotropic decomposition is the easiest way to compute a multidimensional wavelet transform, as it corresponds to applying 1D wavelet decompositions in each direction. In the 2D case, the algorithm is schematized in figure A2.

Let h, g and h^*, g^*, (or $\tilde{h}$, $\tilde{g}$, and $\tilde{h}^*$, $\tilde{g}^*$ respectively) be the low-pass and the high-pass filters corresponding to the scaling function ϕ and the wavelet ψ, and their biorthogonal functions

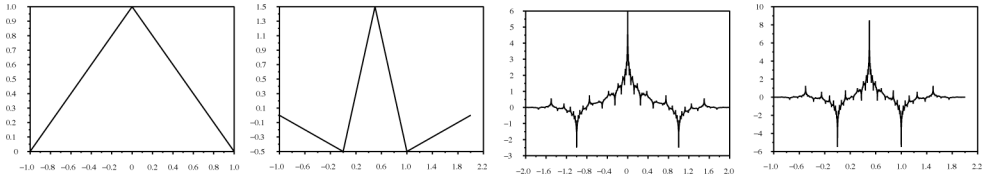

Figure A1. From left to right, the scaling function ϕ with its associated symmetric wavelet with shortest support, and their duals, namely the dual scaling function ϕ^* and the dual wavelet ψ^*.

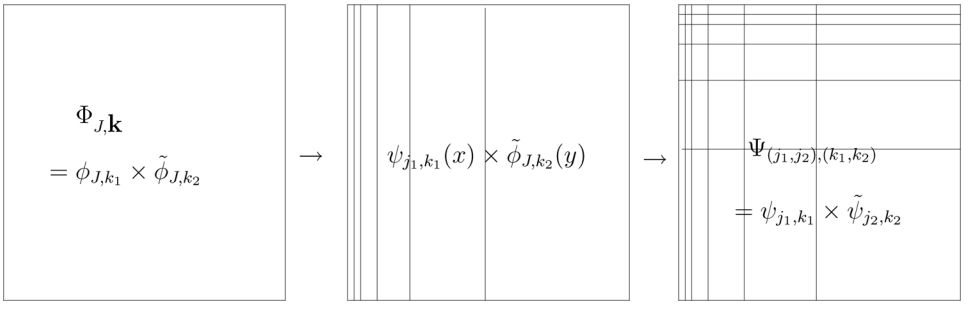

Figure A2. Anisotropic 2D wavelet transform.

ϕ^*, ψ^*(or $\tilde{\phi}$ and $\tilde{\psi}$ and their biorthogonal functions $\tilde{\phi}^*$, $\tilde{\psi}^*$ respectively). We shall note in 'pseudocode' that

$$d^{\mathrm{an}}_{\boldsymbol{j},\boldsymbol{k}} = \mathrm{FWT2\_an}(u, h^*, g^*, \tilde{h}^*, \tilde{g}^*), \tag{A7}$$

which is the 2D anisotropic fast wavelet transform in the periodic case (see [25] for the details of the algorithm) corresponding to the formula

$$d^{\mathrm{an}}_{\boldsymbol{j},\boldsymbol{k}} = \langle u | \Psi^{\mathrm{an},*}_{\boldsymbol{j},\boldsymbol{k}} \rangle,$$

$\Psi^{\mathrm{an},*}_{\boldsymbol{j},\boldsymbol{k}}$ being the dual function of $\Psi^{\mathrm{an}}_{\boldsymbol{j},\boldsymbol{k}}$. Similarly,

$$u = \mathrm{IFWT2\_an}(d^{\mathrm{an}}_{\boldsymbol{j},\boldsymbol{k}}, h, g, \tilde{h}, \tilde{g}) \tag{A8}$$

will denote the inverse transform, which corresponds to the formula

$$u(x, y) = \sum_{\boldsymbol{j},\boldsymbol{k}} d^{\mathrm{an}}_{\boldsymbol{j},\boldsymbol{k}}\ \Psi^{\mathrm{an}}_{\boldsymbol{j},\boldsymbol{k}}(x, y)$$

evaluated at collocation points. Starting from $2^J \times 2^J$ collocation points, the computational cost of the $d^{\mathrm{an}}_{\boldsymbol{j},\boldsymbol{k}}$ is $\mathrm{O}(2^J \times 2^J)$ operations.

In the isotropic case, the 2D wavelets are obtained through tensor products of wavelets and scaling functions or wavelets on the *same* scale. This produces the following basis of $L^2(\mathbb{R})$: $\{\Psi^{\varepsilon}_{j,k} = 2^j \Psi^{\varepsilon}(2^j \boldsymbol{x} - \boldsymbol{k});\ j \in \mathbb{Z},\ \boldsymbol{k} \in \mathbb{Z}^2,\ \varepsilon \in \{(1,0), (0,1), (1,1)\}\}$, where

$$\Psi^{(1,0)}(x, y) = \psi(x)\,\tilde{\phi}(y), \quad \Psi^{(0,1)}(x, y) = \phi(x)\,\tilde{\psi}(y), \quad \Psi^{(1,1)}(x, y) = \psi(x)\,\tilde{\psi}(y).$$

The interest of this basis remains in the fact that the size of their support is proportional to 2^{-j} in each direction, that is, the basis functions are 'isotropic'. The principle of the associated decomposition algorithm is illustrated in figure A3.

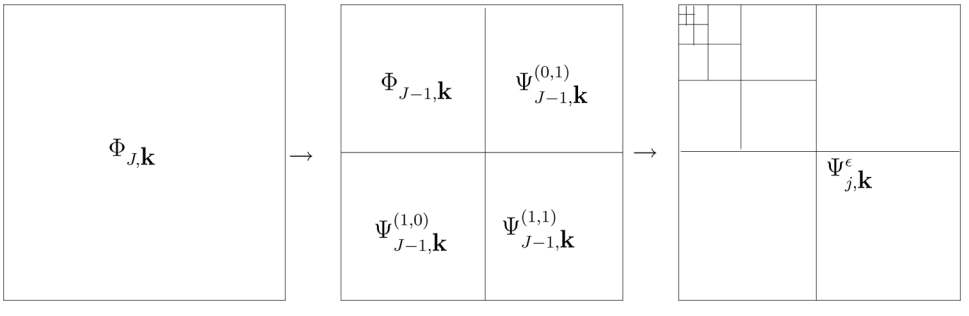

Figure A3. Isotropic 2D wavelet transform.

As for the anisotropic case, we shall note in 'pseudo-code' that

$$d^{\varepsilon}_{j,\boldsymbol{k}} = \mathrm{FWT2}(u, h^*, g^*, \tilde{h}^*, \tilde{g}^*), \tag{A9}$$

which is the 2D isotropic fast wavelet transform in the periodic case (see [25] for the details) corresponding to the formula

$$d^{\varepsilon}_{j,\boldsymbol{k}} = \langle u | \Psi^{\varepsilon,*}_{j,\boldsymbol{k}} \rangle,$$

$\Psi^{\varepsilon,*}_{j,\boldsymbol{k}}$ being the dual function of $\Psi^{\varepsilon}_{j,\boldsymbol{k}}$. Similarly,

$$u = \mathrm{IFWT2}(d^{\varepsilon}_{j,\boldsymbol{k}}, h, g, \tilde{h}, \tilde{g}) \tag{A10}$$

will denote the inverse transform, which corresponds to the formula

$$u(x, y) = \sum_{\varepsilon, j, \boldsymbol{k}} d^{\varepsilon}_{j,\boldsymbol{k}} \, \Psi^{\varepsilon}_{j,\boldsymbol{k}}(x, y)$$

evaluated at collocation points. Starting from $2^J \times 2^J$ collocation points, the computational cost of the $d^{\varepsilon}_{\boldsymbol{j},\boldsymbol{k}}$ is $\mathrm{O}(2^J \times 2^J)$ operations.

Appendix B: Divergence-free wavelet formulae

In this apprendix, we state explicitly the formulae for the 2D and 3D isotropic divergence-free wavelets, and the practical way to compute the associated coefficients.

B.1 *In two dimensions*

The isotropic divergence-free wavelets are elementary combinations of the six generating 2D vector wavelets written in equation (3), namely

$$\begin{cases} \Psi^{(1,0)}_1 \\ \Psi^{(1,0)}_2 \end{cases} \rightarrow \begin{cases} \Psi^{(1,0)}_{\mathrm{div}} = \Psi^{(1,0)}_2 - 1/4\big[\Psi^{(1,0)}_1 - \Psi^{(1,0)}_1(x_1, x_2 - 1)\big], \\ \Psi^{(1,0)}_n = \Psi^{(1,0)}_1, \end{cases}$$

$$\begin{cases} \Psi^{(0,1)}_1 \\ \Psi^{(0,1)}_2 \end{cases} \rightarrow \begin{cases} \Psi^{(0,1)}_{\mathrm{div}} = \Psi^{(0,1)}_1 - 1/4\big[\Psi^{(0,1)}_2 - \Psi^{(0,1)}_2(x_1 - 1, x_2)\big], \\ \Psi^{(0,1)}_n = \Psi^{(0,1)}_2, \end{cases}$$

$$\begin{cases} \Psi^{(1,1)}_1 \\ \Psi^{(1,1)}_2 \end{cases} \rightarrow \begin{cases} \Psi^{(1,1)}_{\mathrm{div}} = \Psi^{(1,1)}_1 - \Psi^{(1,1)}_2, \\ \Psi^{(1,1)}_n = \Psi^{(1,1)}_1 + \Psi^{(1,1)}_2, \end{cases}$$

In the new basis $\{\Psi^{\varepsilon}_{\mathrm{div},j,\boldsymbol{k}}, \ \Psi^{\varepsilon}_{n,j,\boldsymbol{k}}\}$ the expansion of a vector $\boldsymbol{u}$ given by

$$\begin{aligned} \boldsymbol{u} = &\sum_{j \in \mathbb{Z}} \sum_{\boldsymbol{k} \in \mathbb{Z}^2} \left(d^{(1,0)}_{\mathrm{div},j,\boldsymbol{k}} \, \Psi^{(1,0)}_{\mathrm{div},j,\boldsymbol{k}} + d^{(0,1)}_{\mathrm{div},j,\boldsymbol{k}} \, \Psi^{(0,1)}_{\mathrm{div},j,\boldsymbol{k}} + d^{(1,1)}_{\mathrm{div},j,\boldsymbol{k}} \, \Psi^{(1,1)}_{\mathrm{div},j,\boldsymbol{k}} \right) \\ &+ \sum_{j \in \mathbb{Z}} \sum_{\boldsymbol{k} \in \mathbb{Z}^2} \left(d^{(1,0)}_{n,j,\boldsymbol{k}} \, \Psi^{(1,0)}_{n,j,\boldsymbol{k}} + d^{(0,1)}_{n,j,\boldsymbol{k}} \, \Psi^{(0,1)}_{n,j,\boldsymbol{k}} + d^{(1,1)}_{n,j,\boldsymbol{k}} \, \Psi^{(1,1)}_{n,j,\boldsymbol{k}} \right) \end{aligned} \tag{B1}$$

is related to the standard expansion (4) by the relationship between the new coefficients and the original ones $d^{\varepsilon}_{i,j,\boldsymbol{k}}$:

$$(d_{\mathrm{div}})\ \begin{cases} d^{(1,0)}_{\mathrm{div},j,\boldsymbol{k}} = d^{(1,0)}_{2,j,\boldsymbol{k}}, \\ d^{(0,1)}_{\mathrm{div},j,\boldsymbol{k}} = d^{(0,1)}_{1,j,\boldsymbol{k}}, \\ d^{(1,1)}_{\mathrm{div},j,\boldsymbol{k}} = 1/2 d^{(1,1)}_{1,j,\boldsymbol{k}} - 1/2 d^{(1,1)}_{2,j,\boldsymbol{k}}, \end{cases} \qquad (d_n)\ \begin{cases} d^{(1,0)}_{n,j,\boldsymbol{k}} = d^{(1,0)}_{1,j,\boldsymbol{k}} + 1/4 d^{(1,0)}_{2,j,\boldsymbol{k}} - 1/4 d^{(1,0)}_{2,j,k_1,k_2-1}, \\ d^{(0,1)}_{n,j,\boldsymbol{k}} = d^{(0,1)}_{2,j,\boldsymbol{k}} + 1/4 d^{(0,1)}_{1,j,\boldsymbol{k}} - 1/4 d^{(0,1)}_{1,j,k_1-1,k_2}, \\ d^{(1,1)}_{n,j,\boldsymbol{k}} = 1/2 d^{(1,1)}_{1,j,\boldsymbol{k}} + 1/2 d^{(1,1)}_{2,j,\boldsymbol{k}}. \end{cases} \tag{B2}$$

B.2 *In three dimensions*

The MRA $(V^1_j \otimes V^0_j \otimes V^0_j) \times (V^0_j \otimes V^1_j \otimes V^0_j) \times (V^0_j \otimes V^0_j \otimes V^1_j)$ provides naturally three generating *3D-vector scaling functions*, namely

$$\Phi_1(x_1,x_2,x_3) = \begin{vmatrix} \phi_1(x_1)\phi_0(x_2)\phi_0(x_3) \\ 0 \\ 0 \end{vmatrix}, \quad \Phi_2 = \begin{vmatrix} 0 \\ \phi_0\phi_1\phi_0 \\ 0 \end{vmatrix}, \quad \Phi_3 = \begin{vmatrix} 0 \\ 0 \\ \phi_0\phi_0\phi_1 \end{vmatrix},$$

and 21 generating *3D-vector wavelets*, namely

$$\left\{ \Psi^{\epsilon}_i \mid i = 1,2,3\ ,\ \epsilon = (\varepsilon_1,\varepsilon_2,\varepsilon_3) \text{ with } \varepsilon_i = 0,1 \text{ and } \epsilon \neq (0,0,0) \right\}.$$

For example, the expressions for the wavelets $\Psi^{(1,0,0)}_i$, $\Psi^{(1,1,0)}_i$ and $\Psi^{(1,1,1)}_i$ are

$$\Psi^{(1,0,0)}_1(x_1,x_2,x_3) = \begin{vmatrix} \psi_1(x_1)\phi_0(x_2)\phi_0(x_3) \\ 0 \\ 0 \end{vmatrix}, \quad \Psi^{(1,0,0)}_2 = \begin{vmatrix} 0 \\ \psi_0\phi_1\phi_0, \\ 0 \end{vmatrix} \quad \Psi^{(1,0,0)}_3 = \begin{vmatrix} 0 \\ 0 \\ \psi_0\phi_0\phi_1 \end{vmatrix},$$

$$\Psi^{(1,1,0)}_1(x_1,x_2,x_3) = \begin{vmatrix} \psi_1(x_1)\psi_0(x_2)\phi_0(x_3) \\ 0 \\ 0 \end{vmatrix}, \quad \Psi^{(1,1,0)}_2 = \begin{vmatrix} 0 \\ \psi_0\psi_1\phi_0, \\ 0 \end{vmatrix} \quad \Psi^{(1,1,0)}_3 = \begin{vmatrix} 0 \\ 0 \\ \psi_0\psi_0\phi_1 \end{vmatrix},$$

$$\Psi^{(1,1,1)}_1(x_1,x_2,x_3) = \begin{vmatrix} \psi_1(x_1)\psi_0(x_2)\psi_0(x_3) \\ 0 \\ 0 \end{vmatrix}, \quad \Psi^{(1,1,1)}_2 = \begin{vmatrix} 0 \\ \psi_0\psi_1\psi_0, \\ 0 \end{vmatrix} \quad \Psi^{(1,1,1)}_3 = \begin{vmatrix} 0 \\ 0 \\ \psi_0\psi_0\psi_1 \end{vmatrix}.$$

Similar expressions can be obtained from the wavelets associated with the parameters (0, 1, 0), (0, 0, 1), (1, 0, 1) and (0, 1, 1).

Let us introduce $\Omega^*_3 = \{\varepsilon \in \{0,1\}^3 \setminus (0,0,0)\}$. The *isotropic* wavelet expansion of a given 3D vector function $\boldsymbol{u}$ is written in this basis as

$$\boldsymbol{u} = \sum_{j\in\mathbb{Z}} \sum_{\boldsymbol{k}\in\mathbb{Z}^3} \sum_{\varepsilon\in\Omega^*_3} \left(d^{\varepsilon}_{1,j,\boldsymbol{k}}\ \Psi^{\varepsilon}_{1,j,\boldsymbol{k}} + d^{\varepsilon}_{2,j,\boldsymbol{k}}\ \Psi^{\varepsilon}_{2,j,\boldsymbol{k}} + d^{\varepsilon}_{3,j,\boldsymbol{k}}\ \Psi^{\varepsilon}_{3,j,\boldsymbol{k}} \right). \tag{B3}$$

Following section 2.1, there exist 14 kinds of isotropic divergence-free wavelet, with the arbitrary possible choices in equation (2). In the following we do not detail all the expressions;

we choose only some typical expressions:

$$\Psi^{(1,0,0)}_{\mathrm{div},1}(x_1,x_2,x_3) = \begin{vmatrix} -1/4\psi_1(x_1)[\phi_0(x_2)-\phi_0(x_2-1)]\phi_0(x_3) \\ \psi_0(x_1)\phi_1(x_2)\phi_0(x_3) \\ 0 \end{vmatrix},$$

$$\Psi^{(1,0,0)}_{\mathrm{div},2}(x_1,x_2,x_3) = \begin{vmatrix} -1/4\psi_1(x_1)\phi_0(x_2)[\phi_0(x_3)-\phi_0(x_3-1)] \\ 0 \\ \psi_0(x_1)\phi_0(x_2)\phi_1(x_3) \end{vmatrix},$$

$$\Psi^{(1,1,0)}_{\mathrm{div},1}(x_1,x_2,x_3) = \begin{vmatrix} \psi_1(x_1)\psi_0(x_2)\phi_0(x_3) \\ -\psi_0(x_1)\psi_1(x_2)\phi_0(x_3), \\ 0 \end{vmatrix}$$

$$\Psi^{(1,1,0)}_{\mathrm{div},2}(x_1,x_2,x_3) = \begin{vmatrix} -1/8\psi_1(x_1)\psi_0(x_2)[\phi_0(x_3)-\phi_0(x_3-1)] \\ -1/8\psi_0(x_1)\psi_1(x_2)[\phi_0(x_3)-\phi_0(x_3-1)], \\ \psi_0(x_1)\psi_0(x_2)\phi_1(x_3) \end{vmatrix}$$

$$\Psi^{(1,1,1)}_{\mathrm{div},1}(x_1,x_2,x_3) = \begin{vmatrix} -\psi_1(x_1)\psi_0(x_2)\psi_0(x_3) \\ 0 \\ \psi_0(x_1)\psi_0(x_2)\psi_1(x_3) \end{vmatrix},$$

$$\Psi^{(1,1,1)}_{\mathrm{div},2}(x_1,x_2,x_3) = \begin{vmatrix} 0 \\ \psi_0(x_1)\psi_1(x_2)\psi_0(x_3) \\ -\psi_0(x_1)\psi_0(x_2)\psi_1(x_3) \end{vmatrix}.$$

Similar expressions can be obtained for all basis functions: for each $\varepsilon \in \Omega_3^*$ given, two divergence-free wavelets $\Psi^{\varepsilon}_{\mathrm{div},i}$, $i = 1, 2$ are found by linear combination of Ψ^{ε}_1, Ψ^{ε}_2, Ψ^{ε}_3, in order to satisfy the divergence-free condition. The complement wavelet Ψ^{ε}_n is constructed in order to take care of the symmetry. For example, we consider

$$\begin{aligned}
\Psi^{(1,0,0)}_{\mathrm{div},1} &= \Psi^{(1,0,0)}_2 - 1/4(\Psi^{(1,0,0)}_1(.,.,.) - \Psi^{(1,0,0)}_1(.,.-1,.)), \\
\Psi^{(1,0,0)}_{\mathrm{div},2} &= \Psi^{(1,0,0)}_3 - 1/4(\Psi^{(1,0,0)}_1(.,.,.) - \Psi^{(1,0,0)}_1(.,.,.-1)), \\
\Psi^{(1,0,0)}_n &= \Psi^{(1,0,0)}_1,
\end{aligned}$$

also similarly, for $\Psi^{(0,1,0)}_{\mathrm{div},i}$ and $\Psi^{(0,0,1)}_{\mathrm{div},i}$, $i = 1, 2$,

$$\begin{aligned}
\Psi^{(1,1,0)}_{\mathrm{div},1} &= \Psi^{(1,1,0)}_1 - \Psi^{(1,1,0)}_2, \\
\Psi^{(1,1,0)}_{\mathrm{div},2} &= \Psi^{(1,1,0)}_3 - 1/8(\Psi^{(1,1,0)}_1(.,.,.) - \Psi^{(1,1,0)}_1(.,.,.-1)) \\
&\quad -1/8(\Psi^{(1,1,0)}_2(.,.,.) - \Psi^{(1,1,0)}_2(.,.,.-1)), \\
\Psi^{(1,1,0)}_n &= \Psi^{(1,1,0)}_1 + \Psi^{(1,1,0)}_2,
\end{aligned}$$

and similarly, for $\Psi^{(0,1,1)}_{\mathrm{div},i}$ and $\Psi^{(1,0,1)}_{\mathrm{div},i}$, $i = 1, 2$,

$$\begin{aligned}
\Psi^{(1,1,1)}_{\mathrm{div},1} &= \Psi^{(1,1,1)}_3 - \Psi^{(1,1,1)}_1, \\
\Psi^{(1,1,1)}_{\mathrm{div},2} &= \Psi^{(1,1,1)}_2 - \Psi^{(1,1,1)}_3, \\
\Psi^{(1,1,1)}_n &= \Psi^{(1,1,1)}_1 + \Psi^{(1,1,1)}_2 + \Psi^{(1,1,1)}_3.
\end{aligned}$$

Now we can rewrite equation (B3) as

$$\boldsymbol{u} = \sum_{j\in\mathbb{Z}} \sum_{\boldsymbol{k}\in\mathbb{Z}^3} \sum_{\varepsilon\in\Omega_3^*} \left(d^{\varepsilon}_{\mathrm{div},1,j,\boldsymbol{k}} \Psi^{\varepsilon}_{\mathrm{div},1,j,\boldsymbol{k}} + d^{\varepsilon}_{\mathrm{div},2,j,\boldsymbol{k}} \Psi^{\varepsilon}_{\mathrm{div},2,j,\boldsymbol{k}} + d^{\varepsilon}_{n,j,\boldsymbol{k}} \Psi^{\varepsilon}_{n,j,\boldsymbol{k}}\right),$$

where the divergence-free wavelet coefficients are simply obtained from the standard coefficents, for example

$$\begin{cases} d^{(1,0,0)}_{\mathrm{div},1} = d^{(1,0,0)}_{2}, \\ d^{(1,0,0)}_{\mathrm{div},2} = d^{(1,0,0)}_{3} \end{cases},$$

$$\begin{cases} d^{(1,1,0)}_{\mathrm{div},1} = 1/2\left(d^{(1,1,0)}_{1} - d^{(1,1,0)}_{2}\right), \\ d^{(1,1,0)}_{\mathrm{div},2} = d^{(1,1,0)}_{3}, \end{cases}$$

$$\begin{cases} d^{(1,1,1)}_{\mathrm{div},1} = 1/3\left(-2d^{(1,1,1)}_{1} + d^{(1,1,1)}_{2} + d^{(1,1,1)}_{3}\right), \\ d^{(1,1,1)}_{\mathrm{div},2} = 1/3\left(-d^{(1,1,1)}_{1} + 2d^{(1,1,1)}_{2} - d^{(1,1,1)}_{3}\right). \end{cases}$$

The complement coefficients are in this case

$$(d_n) \quad \begin{cases} d^{(1,0,0)}_{n,\boldsymbol{k}} = d^{(1,0,0)}_{1,k_1,k_2,k_3} + 1/4\left(d^{(1,0,0)}_{2,k_1,k_2,k_3} - d^{(1,0,0)}_{2,k_1,k_2-1,k_3}\right), +1/4\left(d^{(1,0,0)}_{3,k_1,k_2,k_3} - d^{(1,0,0)}_{3,k_1,k_2,k_3-1}\right) \\ d^{(1,1,0)}_{n,\boldsymbol{k}} = 1/2\left(d^{(1,1,0)}_{1} + d^{(1,1,0)}_{2}\right) + 1/8\left(d^{(1,1,0)}_{3,k_1,k_2,k_3} - d^{(1,1,0)}_{3,k_1,k_2,k_3-1}\right), \\ d^{(1,1,1)}_{n} = 1/3\left(d^{(1,1,1)}_{1} + d^{(1,1,1)}_{2} + d^{(1,1,1)}_{3}\right). \end{cases}$$

Appendix C: Pseudocode

In this appendix we summarize in pseudocode the algorithms for 2D anisotropic divergence-free and curl-free wavelets. Similar pseudocodes are given for the isotropic case, and for the 3D case.

We start from two MRA (V_j^0) and (V_j^1) with scaling functions ϕ_0, ϕ_1 and wavelets ψ_0, ψ_1 verifying equation (1):

$$\phi_1'(x) = \phi_0(x) - \phi_0(x-1), \quad \psi_1'(x) = 4\,\psi_0(x). \tag{1}$$

Equation (1) can be rewritten for the dual functions ϕ_0^*, ψ_0^*, ϕ_1^*, and ψ_1^*:

$$\phi_0^{*\prime}(x) = \phi_1^*(x+1) - \phi_1^*(x), \quad \psi_0^{*\prime}(x) = -4\,\psi_1^*(x). \tag{C1}$$

For the transfer functions, it can be represented by

$$m_0(\xi) = \frac{2}{1+\mathrm{e}^{-\mathrm{i}\xi}}\, m_1(\xi), \quad m_0^*(\xi) = \frac{1+\mathrm{e}^{\mathrm{i}\xi}}{2}\, m_1^*(\xi). \tag{C2}$$

The transfer functions corresponding to the spline of degree 1 and 2 degree of figure 1 are given by [23, 24]:

$$m_0(\xi) = \mathrm{e}^{\mathrm{i}\xi}\left(\frac{1+\mathrm{e}^{-\mathrm{i}\xi}}{2}\right)^2, \quad m_1(\xi) = \mathrm{e}^{\mathrm{i}\xi}\left(\frac{1+\mathrm{e}^{-\mathrm{i}\xi}}{2}\right)^3, \tag{C3}$$

leading to the values for the decomposition and reconstruction filters given in table 1:

C.1 *Direct and inverse two-dimensional anisotropic divergence, free wavelet transforms*

The notation and formulae are given in section 3.2.1. We suppose that we are given a 2D periodic field $(u_1(x_1, x_2), u_2(x_1, x_2))$ known at collocation points $\{2^{-J}\,\boldsymbol{k},\ \boldsymbol{k} \in [0, 2^{-J} - 1]^2\}$.

C.1.1 Direct transform

$$\tilde{d}_{1,\boldsymbol{j},\boldsymbol{k}} = \text{FWT2\_an}(u_1, h^{*1}, g^{*1}, h^{*0}, g^{*0}),$$
$$\tilde{d}_{2,\boldsymbol{j},\boldsymbol{k}} = \text{FWT2\_an}(u_2, h^{*0}, g^{*0}, h^{*1}, g^{*1});$$

for $\boldsymbol{j} = (j_1, j_2)$, and for $\boldsymbol{k}$,

$$d_{1,\boldsymbol{j},\boldsymbol{k}} = 2^{(j_1+j_2)/2}\tilde{d}_{1,\boldsymbol{j},\boldsymbol{k}},$$
$$d_{2,\boldsymbol{j},\boldsymbol{k}} = 2^{(j_1+j_2)/2}\tilde{d}_{2,\boldsymbol{j},\boldsymbol{k}}.$$

(Renormalization $L^2 \to L^\infty$ of the coefficients)

$$d_{\text{div},\boldsymbol{j},\boldsymbol{k}} = \frac{2^{j_2}}{2^{2j_1} + 2^{2j_2}}\, d_{1,\boldsymbol{j},\boldsymbol{k}} - \frac{2^{j_1}}{2^{2j_1} + 2^2 j_2}\, d_{2,\boldsymbol{j},\boldsymbol{k}},$$
$$d_{n,\boldsymbol{j},\boldsymbol{k}} = \frac{2^{j_1}}{2^{2j_1} + 2^{2j_2}}\, d_{1,\boldsymbol{j},\boldsymbol{k}} + \frac{2^{j_2}}{2^{2j_1} + 2^{2j_2}}\, d_{2,\boldsymbol{j},\boldsymbol{k}},$$

end.

In the periodic case, one has to take care of the role played by the 1D scaling function $\phi = 1$ in the 2D anisotropic wavelet basis, and to adapt the above formulae for the corresponding coefficients.

The $d_{\text{div},\boldsymbol{j},\boldsymbol{k}}$ are the divergence-free wavelet coefficients of $\boldsymbol{u}$. Note that, if $\boldsymbol{u}$ is divergence free, one obtains $d_{n,\boldsymbol{j},\boldsymbol{k}} = 0$ (and these coefficients do not need to be computed).

C.1.2 Inverse transform. Starting from the coefficients $d_{\text{div},\boldsymbol{j},\boldsymbol{k}}$ and $d_{n,\boldsymbol{j},\boldsymbol{k}}$ we have the following:
for $\boldsymbol{j} = (j_1, j_2)$, and for $\boldsymbol{k}$,

$$d_{1,\boldsymbol{j},\boldsymbol{k}} = 2^{j_2}\, d_{\text{div},\boldsymbol{j},\boldsymbol{k}} + 2^{j_1}\, d_{n,\boldsymbol{j},\boldsymbol{k}},$$
$$d_{2,\boldsymbol{j},\boldsymbol{k}} = -2^{j_1}\, d_{\text{div},\boldsymbol{j},\boldsymbol{k}} + 2^{j_2}\, d_{n,\boldsymbol{j},\boldsymbol{k}},$$
$$\tilde{d}_{1,\boldsymbol{j},\boldsymbol{k}} = 2^{-(j_1+j_2)/2} d_{1,\boldsymbol{j},\boldsymbol{k}},$$
$$\tilde{d}_{2,\boldsymbol{j},\boldsymbol{k}} = 2^{-(j_1+j_2)/2} d_{2,\boldsymbol{j},\boldsymbol{k}},$$

end

$$u_1 = \text{IFWT2\_an}(\tilde{d}_{1,\boldsymbol{j},\boldsymbol{k}}, h^1, g^1, h^0, g^0),$$
$$u_2 = \text{IFWT2\_an}(\tilde{d}_{2,\boldsymbol{j},\boldsymbol{k}}, h^0, g^0, h^1, g^1).$$

C.2 *Direct and inverse two-dimensional anisotropic curl-free wavelet transforms*

The curl-free wavelet transform provides formulae identical with the divergence-free transform (see section 4.2), except that one has to permutate the role of V_j^0 and V_j^1, replacing d_n by d_{curl}, and d_{div} by d_N.

C.2.1 Direct transform. Starting from $\boldsymbol{u} = (u_1, u_2)$ at collocation points,

$$\tilde{d}_{1,\boldsymbol{j},\boldsymbol{k}} = \text{FWT2\_an}(u_1, h^{*0}, g^{*0}, h^{*1}, g^{*1}),$$
$$\tilde{d}_{2,\boldsymbol{j},\boldsymbol{k}} = \text{FWT2\_an}(u_2, h^{*1}, g^{*1}, h^{*0}, g^{*0});$$

for $\boldsymbol{j} = (j_1, j_2)$, and for $\boldsymbol{k}$,

$$d_{1,\boldsymbol{j},\boldsymbol{k}} = 2^{(j_1+j_2)/2}\tilde{d}_{1,\boldsymbol{j},\boldsymbol{k}},$$
$$d_{2,\boldsymbol{j},\boldsymbol{k}} = 2^{(j_1+j_2/2)}\tilde{d}_{2,\boldsymbol{j},\boldsymbol{k}},$$

(Renormalization $L^2 \to L^\infty$ of the coefficients)

$$d_{\text{curl},\boldsymbol{j},\boldsymbol{k}} = \frac{2^{j_1}}{2^{2j_1}+2^{2j_2}}\, d_{1,\boldsymbol{j},\boldsymbol{k}} + \frac{2^{j_2}}{2^{2j_1}+2^{2j_2}}\, d_{2,\boldsymbol{j},\boldsymbol{k}},$$
$$d_{N,\boldsymbol{j},\boldsymbol{k}} = \frac{2^{j_2}}{2^{2j_1}+2^{2j_2}}\, d_{1,\boldsymbol{j},\boldsymbol{k}} - \frac{2^{j_1}}{2^{2j_1}+2^{2j_2}}\, d_{2,\boldsymbol{j},\boldsymbol{k}},$$

end.

The $d_{\text{curl},\boldsymbol{j},\boldsymbol{k}}$ are the curl-free wavelet coefficients of $\boldsymbol{u}$. Note that, if $\boldsymbol{u}$ is curl free, one obtains $d_{N,\boldsymbol{j},\boldsymbol{k}} = 0$.

C.2.2 Inverse transform Starting from the coefficients $d_{\text{curl},\boldsymbol{j},\boldsymbol{k}}$ and $d_{N,\boldsymbol{j},\boldsymbol{k}}$ we have the following.
for $\boldsymbol{j} = (j_1, j_2)$, and for $\boldsymbol{k}$,

$$d_{1,\boldsymbol{j},\boldsymbol{k}} = 2^{j_2}\, d_{N,\boldsymbol{j},\boldsymbol{k}} + 2^{j_1}\, d_{\text{curl},\boldsymbol{j},\boldsymbol{k}},$$
$$d_{2,\boldsymbol{j},\boldsymbol{k}} = -2^{j_1}\, d_{N,\boldsymbol{j},\boldsymbol{k}} + 2^{j_2}\, d_{\text{curl},\boldsymbol{j},\boldsymbol{k}}$$
$$\tilde{d}_{1,\boldsymbol{j},\boldsymbol{k}} = 2^{-(j_1+j_2)/2} d_{1,\boldsymbol{j},\boldsymbol{k}}$$
$$\tilde{d}_{2,\boldsymbol{j},\boldsymbol{k}} = 2^{-(j_1+j_2)/2} d_{2,\boldsymbol{j},\boldsymbol{k}},$$

end

$$u_1 = \text{IFWT2\_an}(\tilde{d}_{1,\boldsymbol{j},\boldsymbol{k}}, h^0, g^0, h^1, g^1),$$
$$u_2 = \text{IFWT2\_an}(\tilde{d}_{2,\boldsymbol{j},\boldsymbol{k}}, h^1, g^1, h^0, g^0).$$

Acknowledgments

The authors would like to thank G.-H. Cottet and G. Lapeyre for helpfully providing them with numerical turbulent flows for analyses. This work has been supported in part by the European Community's Improving Human Potential Programme under contract HPRN-CT-2002-00286, 'Breaking complexity.'

References

[1] Farge, M., 1992, Wavelet transforms and their applications to turbulence. Annual Review of Fluid Mechanics, **24**, 395–457.

[2] Meneveau, C., 1991, Analysis of turbulence in the orthonormal wavelet representation. *Journal of Fluid Mechanics*, **232**, 469–520.

[3] Lewalle, J., 1993, Wavelet transform of the Navier–Stokes equations and the generalized dimensions of turbulence. *Applied Scientific Research*, **51**, 109–113.
[4] Charton, P. and Perrier, V., 1996, A pseudo-wavelet scheme for the two-dimensional Navier–Stokes equations. *Computational and Applied Mathematics*, **15**, 139–160.
[5] Fröhlich J. and Schneider, K., 1996, Numerical simulation of decaying turbulence in an adaptive wavelet basis. *Applied and Computational Harmonic Analysis*, **3**, 393–397.
[6] Farge, M., Kevlahan, N., Perrier V. and Goirand, E., 1996, Wavelets and turbulence. *Proceedings of the IEEE*, **84**, 639–669.
[7] Schneider, K., Kevlahan, N. and Farge, M., 1997, Comparison of an adaptive wavelet method and nonlinearly filtered pseudo-spectral methods for two-dimensional turbulence. *Theoretical and Computational Fluid Dynamiccs*, **9**, 191–206.
[8] Koster, F., Griebel, M., Kevlahan, N., Farge M. and Schneider, K., 1998, Towards an adaptive wavelet-based 3D Navier–Stokes solver. In: E.H. Hirschel (Ed.), *Numerical Flow Simulation* I, Notes on Numerical Fluid Mechanics, vol. 66, Braunschweig: Vieweg, pp. 339–364.
[9] Griebel, M. and Koster, F., 2000, Adaptive wavelet solvers for the unsteady incompressible Navier–Stokes equations, In: J. Malek and J. Necas and M. Rokyta (Eds), *Advances in Mathematical Fluid Mechanics* (Berlin: Springer).
[10] Kevlahan, N., Vasilyev, O.V., Goldstein, D. and Jay, A., 2004, A three-dimensional adaptive wavelet method for fluid–structure interaction. In: B. J. Geurts, R. Friedrich and O. Métais (Eds) *Direct and Large-Eddy Simulation V* (Dordrecht: Kluwer), 8 pp.
[11] Kevlahan, N.K.-R. and Vasilyev, O.V., 2005, An adaptive wavelet collocation method for fluid–structure interaction at high Reynolds numbers. SIAM *Journal on Scientific Computing*, **6**, 1894–1915.
[12] Farge, M. and Schneider, K., 2001, Coherent vortex simulation (CVS), a semi-deterministic turbulence model using wavelets. *Flow, Turbulence and Combustion*, **66**, 393–426.
[13] Goldstein, D., Vasilyev, O. and Kevlahan, N.K.-R., 2004, Adaptive LES of 3D decaying isotropic turbulence. In: P. Moin, N. Mansour and P. Bradshaw (Eds.) *Studying Turbulence Using Numerical Simulation Databases—X, Proceedings of the 2004 Summer Program* (Stanford, CA: Center for Turbulence Research).
[14] Grossmann S. and Löhden, M., 1996, Wavelet analysis of Navier–Stokes flow. *Zeitschrift für Physile B*, **100**, 137–147.
[15] Lemarié-Rieusset, P.G., 1992, Analyses multi-résolutions non orthogonales, commutation entre projecteurs et dérivation et ondelettes vecteurs à divergence nulle. *Revista Matemática Iberoamericana*, **8**, 221.
[16] Albukrek, C.-M., Urban, K., Dahmen, W., Rempfer, D. and Lumley, J.-L., 2002, Divergence-free wavelet analysis of Turbulent Flows. *Journal of Scientific Computing*, **17**, 49–66.
[17] Ko, J., Kurdila, J.A. and Rediniotis, O.K., 2000, Divergence-free bases and multiresolution methods for reduced-order flow modeling. *AIAA Journal*, **38**, 2219–2232.
[18] Urban, K., 2002, *Wavelets in Numerical Simulation* (Berlin: Springer).
[19] Urban, K., 1994, A wavelet-galerkin algorithm for the driven–cavity–Stokes problem in two space dimensions. In: M. Feistauer, R. Rannacher, K. Kozel (Eds), *Numerical Modelling in Continuum Mechanics*, Charles: University Prague, pp. 278–289.
[20] Urban, K., 1996, Using divergence-free wavelets for the numerical solution of the Stokes problem. In: *Proceedings of the Conference on Algebraic Multilevel Iteration Methods with Applications*, Vol. 2, University of Nijmegen, The Netherlands, pp. 261–277.
[21] Dahmen, W., Kunoth, A. and Urban, K., 1996, A wavelet-Galerkin method for the Stokes problem. *Computing*, **56**, 259–302.
[22] Urban, K., 2000, Wavelet Bases in H(div) and H(curl). *Mathematics of Computation*, **70**, 739–766.
[23] Daubechies, I., 1992, *Ten Lectures on Wavelets*, (Philadelphia, Pennsylvania: SIAM).
[24] Kahane, J.-P. and Lemarié-Rieusset, P.G., 1995, *Fourier Series and Wavelets*, London: Gordon and Breach.
[25] Mallat, S., 1998, *A Wavelet Tour of Signal Processing*. New York: Academic Press.
[26] Cohen, A., 2000, Wavelet methods in numerical analysis. *Handbook of Numerical Analysis*, Vol. VII. In: P.G. Ciarlet and J.L.Lions (Eds) Amsterdam: Elsevier.
[27] Girault, V. and Raviart, P.A., 1986, *Finite Element Methods for Navieer–Stokes Equations* (Berlin: Springer).
[28] Chorin, A.J. and Marsden, J.E., 1993, *A Mathematical Introduction to Fluid Mechanics*, 3rd edition (Berlin: Springer).
[29] Bernardi, C. and Maday, Y., 1992, Approximations spectrales de problèmes aux limites elliptiques. *Mathématiques & Applications*, Vol. 10 (Paris: Springer).
[30] De Boor, C., 2001, *A Practical Guide to Splines* (New York: Springer).
[31] Hua, B.L. and Klein, P, 1998, An exact criterion for the stirring properties of nearly two-dimensional turbulence, *Physica D*, **113**, 98–110.
[32] Lapeyre, G., 2000, Topologie de mélange dans un fluide turbulent géophysique. Thèse de doctorat, L'Université Paris VI.
[33] Cottet, G.-H., Michaux, B., Ossia, S. and Vanderlinden, G., 2002, A comparison of spectral and vortex methods in three-dimensional incompressible flows. *Journal of Computational Physics*, **175**, 1–11.
[34] Chiavassa, G. and Liandrat, J., 1997, On the effective construction of compactly supported wavelets satisfying boundary conditions on the interval. *Applied and Computational Harmonic Analysis*, **4**, 62–73.
[35] Monasse, P. and Perrier, V., 1998, Orthonormal wavelet bases adapted for partial differential equations with boundary conditions. SIAM *Journal on Mathematical Analysis*, **29**, 1040–1065.

[36] Cohen, A., Daubechies, I. and Feauveau, J.C., 1992, Biorthogonal bases of compactly supported wavelets. *Communications in Pure and Applied Mathematics*, **45**, 485–560.
[37] Schneider, K. and Farge, M., 2000, *Numerical simulation of a mixing layer in an adaptive wavelet basis*, *Comptes Rendus de l'Academie des Sciences*, *Série II*, 263–269.
[38] Lemarié-Rieusset, P.G., 1994, Un théorème d'inexistance pour les ondelettes vecteurs à divergence nulle. *Comptes Reaches de l'Academie des Sciences*, Série I, **319**, 811–813.
[39] Vasilyev, O.V. and Kevlahan, N.K.-R., 2005, An adaptive multilevel wavelet collocation method for elliptic problems. *Journal Computational Physics* (to be published).